

This item is the archived peer-reviewed author-version of:

Reprogramming of glucocorticoid receptor function by hypoxia

Reference:

Vanderhaeghen Tineke, Timmermans Steven, Watts Deepika, Paakinaho Ville, Eggermont Melanie, Vandewalle Jolien, Wallaeyls Charlotte, Van Wyngene Lise, Van Looveren Kelly, Nuyttens Louise, ...- Reprogramming of glucocorticoid receptor function by hypoxia
EMBO reports / EMBO - ISSN 1469-3178 - (2021), e53083
Full text (Publisher's DOI): <https://doi.org/10.15252/EMBR.202153083>
To cite this reference: <https://hdl.handle.net/10067/1835080151162165141>

Reprogramming of glucocorticoid receptor function by hypoxia.

Tineke Vanderhaeghen^{1,2}, Steven Timmermans^{1,2}, Deepika Watts^{3,4}, Ville Paakinaho⁵, Melanie Eggermont^{1,2}, Jolien Vandewalle^{1,2}, Charlotte Wallaey^{1,2}, Lise Van Wyngene^{1,2}, Kelly Van Looveren^{1,2}, Louise Nuyttens^{1,2}, Sylviane Dewaele^{1,2}, Joke Vanden Berghe^{1,2}, Kelly Lemeire^{1,2}, Joey De Backer⁶, Laura Dirx⁶, Wim Vanden Berghe⁶, Guy Caljon⁶, Bart Ghesquière^{7,8}, Karolien De Bosscher^{9,10}, Ben Wielockx^{3,4}, Jorma J. Palvimo⁵, Rudi Beyaert^{1,2} and Claude Libert^{1,2,*}

¹ VIB Center for Inflammation Research, 9000 Ghent, Belgium.

² Department of Biomedical Molecular Biology, Ghent University, 9000 Ghent, Belgium.

³ Department of Clinical Pathobiochemistry, Institute for Clinical Chemistry and Laboratory Medicine, Technische Universität Dresden, 01307 Dresden, Germany

⁴ DFG Research Centre and Cluster of Excellence for Regenerative Therapies Dresden, Technische Universität Dresden, 01307 Dresden, Germany

⁵ Institute of Biomedicine, University of Eastern Finland, 70211 Kuopio, Finland

⁶ Department of Biomedical Sciences, University of Antwerp, Universiteitsplein, 2610 Wilrijk, Belgium

⁷ Metabolomics Expertise Center, Center for Cancer Biology, VIB Center for Cancer Biology, 3000 Leuven, Belgium

⁸ Metabolomics Expertise Center, Department of Oncology, Katholieke Universiteit Leuven, 3000 Leuven, Belgium

⁹ Translational Nuclear Receptor Research lab, VIB Center for Medical Biotechnology, 9000 Ghent, Belgium.

¹⁰ Department of Biomolecular Medicine, Ghent University, 9000 Ghent, Belgium.

*Corresponding author: Claude Libert, claude.libert@irc.vib-ugent.be

Abstract

Here, we investigate the impact of hypoxia on the hepatic response of glucocorticoid receptor (GR) to dexamethasone (DEX) in mice via RNA-sequencing. Hypoxia causes three types of reprogramming of GR: (i) much weaker induction of classical GR response genes by DEX in hypoxia (ii) a number of genes is induced by DEX specifically in hypoxia and (iii) hypoxia induces a group of genes via activation of the hypothalamic-pituitary-adrenal (HPA) axis. Transcriptional profiles are reflected by changed GR-DNA binding as measured by ChIP sequencing. The HPA axis is induced by hypothalamic HIF1 α and HIF2 α activation and leads to GR-dependent lipolysis and ketogenesis. Acute inflammation, induced by lipopolysaccharide, is prevented by DEX in normoxia but not during hypoxia, and this is attributed to HPA axis activation by hypoxia. We unfold new physiological pathways that have consequences for patients suffering from GC resistance.

Key Words: Crosstalk/Hypoxia/Inflammation/Mechanism/Metabolism

Introduction

Glucocorticoids (GCs) are the major stress hormones, produced by the hypothalamic-pituitary-adrenal (HPA) axis. The production of GCs is initiated by stress, which activates the expression of corticotropin releasing hormone (CRH) in the hypothalamus, leading to the secretion of adrenocorticotrophic hormone (ACTH) by the pituitary in the blood which stimulates the adrenals (Spiga *et al*, 2014). GCs are mainly generated by the adrenal glands and regulate carbohydrate, lipid and protein metabolism (Vegiopoulos & Herzig, 2007; Rose *et al*, 2010). They bind to the intracellular GC receptor (GR), a versatile transcription factor involved in a range of physiological responses. GR can directly regulate the expression of hundreds of genes, many of which have strong anti-inflammatory effects, via DNA binding e.g. in hepatocytes and white blood cells. GR additionally interacts with and prevents the activity of other transcription factors, such as nuclear factor κ B (NF- κ B) (Timmermans *et al*, 2019).

In animal models, inhibition of GC production by surgical adrenalectomy, or inhibition of GR using RU486 (Dejager *et al*, 2010) or via genetic ablation (Kleiman *et al*, 2012) leads to extreme sensitivity for inflammatory stimuli, e.g. in lipopolysaccharide (LPS)-induced endotoxemia. Synthetic GCs, such as dexamethasone (DEX), are widely used in inflammatory diseases like rheumatoid arthritis (RA) (Vandewalle *et al*, 2018), and recently shown to reduce mortality in patients seriously ill with COVID-19 (Sterne *et al*, 2020). We and others have found that the transcriptional induction of genes with anti-inflammatory effects (e.g. *Tsc22d3* encoding Glucocorticoid Induced Leucine Zipper, GILZ, or *Dusp1* encoding Map Kinase Phosphatase 1, MKP1) by GR in organs, such as liver, can become compromised by a mechanism that still needs to be unfolded. In acute, lethal inflammation, like septic shock, a functional decline of GR has been observed and has been called GC resistance (GCR)(Van Bogaert *et al*, 2011; Dendoncker *et al*, 2019; Vandewalle *et al*, 2021). Since the reduction of GR function is possibly the result of interference between transcription factors, certain authors have focused their attention on NF- κ B as a factor responsible for GCR (Dendoncker *et al*, 2019). However, under drastic inflammatory conditions, also hypoxia-induced factors (HIFs), are activated in tissues (Cummins *et al*, 2016). Next to its anti-inflammatory function, GR has important metabolic functions. In fat tissue, GR can activate lipolysis, leading to the release of free fatty acids (FFAs) and glycerol (de Guia & Herzig, 2015). GR also stimulates gluconeogenesis in hepatocytes (Rose & Herzig, 2013). Moreover, GR can play a role in the maturation of the skin barrier (Sevilla & Pérez, 2018) and the lung (Daniel Bird *et al*, 2015) during development.

Hypoxia has an important physiological role during normal life, and the liver is essential for the physiological regulation of gene expression during hypoxia (Jungermann & Kietzmann, 2000). The

major pathway regulating the response to low oxygen (O₂) concentrations involves the activation of HIFs, heterodimeric factors composed of HIF α (mainly HIF1 α and HIF2 α) and HIF β . While the β -subunit is constitutively expressed, HIF α subunits are hydroxylated by the O₂ sensors prolyl-4-hydroxylases (PHDs) in normoxia (Wielockx & Meneses, 2016; Nakayama & Kataoka, 2019). This leads to the binding of the von Hippel-Lindau protein (pVHL) and degradation by the 26S proteasome (Cockman *et al*, 2000; Schofield & Ratcliffe, 2004). In low O₂ concentrations, PHDs lose their enzymatic activity, HIF α is stabilized and translocates to the nucleus. Together with HIF β and other co-factors, they will bind to hypoxia responsive elements (HREs) in the promoter/enhancer of a selection of genes and regulate their expression, mostly by inducing transcription (Wielockx & Meneses, 2016). This is important for the activation of metabolic pathways involved in cellular glucose (Semenza, 2011), lipid metabolism (Mylonis *et al*, 2019) and erythropoiesis (Franke *et al*, 2013). Sensory systems have developed to detect environmental O₂ concentrations and to adapt to hypoxia (Bleymehl *et al*, 2016; Chang *et al*, 2015). When rats are exposed to perinatal hypoxia, *Crh* mRNA levels are significantly higher in the paraventricular nucleus (PVN) of hypothalamic cells (Raff *et al*, 2007) and an age-dependent ACTH and GC response is induced (Bruder *et al*, 2008). The administration of DMOG (dimethylxalylglycine), a PHD inhibitor leading to increased HIF1 α protein levels, elevates plasma GC levels in rats following an acute stressor such as air puffs (Harrell *et al*, 2015). The cortisol awakening response (CAR) in humans, a marker for the HPA axis function, is significantly higher when ascending to an altitude > 3000 m compared to natives residing permanently at high altitude (Park *et al*, 2014). Altogether, hypoxia is able to activate the HPA axis and induce the production of GCs.

Several *in vitro* studies present an interaction between GR and HIF. Kodama *et al*. have identified that a ligand-dependent activation of GR increases hypoxia-dependent gene expression and HRE activity in HeLa cells (Kodama *et al*, 2003). Next, hypoxia causes a transcriptional upregulation of *Nr3c1* in human renal proximal tubular epithelial cells (Leonard *et al*, 2005) and mouse pituitary AtT-20 cells (Zhang *et al*, 2015). In contrast to the previous results, the expression of HIF1 α target genes is decreased in hypoxic HEPG2 cells when stimulated with DEX (Wagner *et al*, 2008). These contradictory findings illustrate highly dynamic interactions between O₂ concentrations and GR function mediated through HIF1 α . Recently, it has been shown that hypoxia is involved in the rewiring of the GR *cistrome*, thereby indicating a reprogramming of the GR to changes in O₂ concentrations (Yang *et al*, 2020). Furthermore, the GR function is essential in oxygen deprived conditions for the expansion of immature erythroid cells during stress erythropoiesis by increasing the erythrocyte count, haematocrit and haemoglobin content of the peripheral blood (Bauer *et al*, 1999). Also *in vivo* studies in zebrafish *larvae* have found a crosstalk between HIF and GR (Vettori *et*

al, 2017; Marchi *et al*, 2020). Although these papers are very valuable, we are convinced that we need to understand the impact of hypoxia on GR in a pathophysiological context *in vivo*.

Severe inflammatory conditions, such as systemic inflammatory response syndrome (SIRS) and sepsis are associated with increased blood lactate levels (Garcia-alvarez *et al*, 2014) and lead to GCR (Dendoncker *et al*, 2019; Van Bogaert *et al*, 2011; Vandewalle *et al*, 2021). Since HIFs are also activated during inflammation (Cummins *et al*, 2016), we investigated whether hypoxia has an impact on the transcriptional activity of GR, and if it accounts for (part of) the GCR. To study this, we compared the response of mice under normoxic conditions (21% O₂) with mice under hypoxia (7% O₂) and studied the genome-wide transcriptional response to DEX and GR DNA-binding profile, in liver. Also, the effect of hypoxia on the HPA axis activation and the metabolite profile in the blood were studied.

Results

Hypoxia modifies the GR response to DEX in the liver

To study the induction of HIF activity in mouse liver during hypoxia, mice were hydrodynamically injected in the tail vein with PBS or with a HRE-driven luciferase reporter plasmid (HRE-luc) and were randomly assigned to normoxia (21% O₂) or hypoxia (7% O₂) (**Fig 1A**). Luciferase activity was measured. In normoxia, we detected a low signal in livers of mice injected with the reporter plasmid. Hypoxia strongly increased the luciferase activity, especially at the 6h and 24h time point (**Fig 1B, C**). A transfection efficiency of about 50% of the HRE-luc reporter plasmid was observed (**Appendix Fig S1A, B**). To investigate the role of HIF1 α and HIF2 α in the regulation of HRE-luc during hypoxia (6h), the reporter activity was measured in HIF1a^{AlbKO} and HIF2a^{AlbKO} mice and was found to be reduced in HIF1a^{AlbKO} mice and absent in HIF2a^{AlbKO} mice, when subjected to hypoxia (**Fig 1D-G**).

We investigated the effect of hypoxia on GR activity by injecting mice i.p. with PBS or DEX (10 mg/kg) after 6h or 24h of normoxia or hypoxia. Since the liver is essential in the physiological regulation of gene expression during hypoxia (Jungermann & Kietzmann, 2000) and since the GR has important metabolic and anti-inflammatory functions in this organ (de Guia & Herzig, 2015; Rose & Herzig, 2013), we isolated livers and performed genome-wide transcriptomics analysis by RNA-seq 2h after PBS or DEX injection (**Fig 2A**). Of the 462 genes that were significantly upregulated by DEX in normoxia (log fold change [LFC] > 1 and P < 0.05), only 220 were upregulated 6h after hypoxia. Also, in normoxia, 394 genes were significantly downregulated by DEX (LFC < -1 and P < 0.05), while only 152 genes were downregulated by DEX after 6h hypoxia (**Fig 2B**). Similarly, only 182 genes were upregulated by DEX 24h after hypoxia, while 476 genes were upregulated by DEX in normoxia. 383 genes were significantly downregulated by DEX in normoxia, while only 143 genes were downregulated by DEX after 24h of hypoxia (**Fig 2D**). When plotting the LFC of all DEX responsive genes (LFC > 1 and P < 0.05 and LFC < -1 and P < 0.05, compared to PBS) in normoxia and hypoxia, a clear reduction of the GR response was observed under hypoxic conditions, both after 6h (**Fig 2C**, slope \pm standard error of linear regression curve (LRC) = 0.6248 \pm 0.007096) and 24h (**Fig 2E**, slope of LRC = 0.5679 \pm 0.007065). Representative examples of GR responsive genes are shown after DEX stimulation in normoxia and hypoxia based on the RNA-seq data (**Fig 2F and 2G**). So, under hypoxic conditions less genes are differentially expressed by DEX, and the fold induction of genes induced/repressed by DEX in hypoxia is less outspoken. Using Enrichr, we compared the pathways controlled by the genes induced by DEX in normoxia alone [6h (n=262) and 24h (n=294)] with those induced by DEX in both normoxia and hypoxia [6h (n=220) and 24h (n=182)]. Based on the 'Wiki

Pathways 2019 Mouse' function in Enrichr, we suggest a shift from inflammation control to metabolic control (**Table 1**).

To explore the mechanism by which hypoxia changes the response of the GR to DEX, we investigated key aspects of the GR signalling in hypoxic conditions. Both after 6h and 24h of hypoxia, the GR protein levels were not declined in the liver (**Fig EV1A**). Subsequently, we studied the effect of hypoxia on GR chromatin-binding by means of genome-wide ChIP-seq. Liver samples were isolated as in RNA-seq (**Fig 2A**): 2h after PBS or DEX stimulation, 6h or 24h after normoxia and hypoxia. Biological triplicates were used for all conditions, given a total of 18 analysed samples (3 N_PBS, 3 N_DEX, 3 H_PBS_6h, 3 H_DEX_6h, 3 H_PBS_24h and 3 H_DEX_24h) and input controls. In **Fig EV1B**, the PCA plot clarifies the variance within samples per condition, based on the peaks found in the ChIP-seq after normalization and scaling of the data. All samples are clustered together per group, except for one sample within the H_PBS_6h group. However, this inconsistency is not problematic since most of the comparisons are based on the DEX stimulated conditions. When plotting the LFC of genes that responded to DEX regardless of their O₂ concentration, we observed a clear DEX effect in normoxia. A reduced DEX effect on GR chromatin-binding was detected both after 6h and 24h of hypoxia (**Fig 2H**). We found that the coverage of the GR DNA-binding peaks, as found after DEX stimulation in normoxia, was generally lower in hypoxia after DEX stimulation, both at the 6h and 24h time points (**Fig 2I**). By means of illustration, GR peaks found at the promoter region of *Fam107a* and *Sgk1* are shown (**Fig EV1D, E**). **Fig EV1C** represents a heatmap based on the GR DNA-binding peaks after normalization and scaling of the ChIP-seq data found in normoxia after DEX stimulation compared to input samples of this group. Log₁₀ of the total area under the peak is displayed in this heatmap. Overall, we observed that the total area under the peak was higher after DEX stimulation compared to PBS both in normoxia and hypoxia (6h and 24h). Additionally, the coverage of GR DNA-binding peaks after DEX stimulation in hypoxia is highly correlated with the peak coverage in the liver of DEX stimulated mice in normoxia [Pearson correlation coefficient (PCC): N_DEX vs H_DEX_6h = 0.9238885 and N_DEX vs H_DEX_24h = 0.914772]. When we only compare the PBS treated groups in normoxia and hypoxia, the GR-DNA binding profile is mostly altered after 6h hypoxia (PCC: N_PBS vs H_PBS_6h = 0.8191357 and N_PBS vs H_PBS_24h = 0.9431441).

To gain insight into the role of HIF in the expression of these GR responsive genes during hypoxia, we examined the expression of *Hspa1a* in the liver of HIF1aHIF2a^{AlbKO} mice and wild-type littermates after 6h hypoxia and DEX stimulation via RT-qPCR. The expression pattern of *Hspa1a* is similar in HIF1aHIF2a^{fl/fl} and HIF1aHIF2a^{AlbKO} mice (**Fig EV1F**). Taken together, these data demonstrate that the reduced GR response to DEX in hypoxia can be linked to a reduced GR DNA-binding (**Fig 2I**), but the changes are largely locus-specific and not observed to the same degree at every GR peak and gene

detected via ChIP-seq. Furthermore, it seems that HIF1 α and HIF2 α in the liver are not involved in the reduced GR response to DEX upon hypoxia.

Expression of specific DEX responsive genes only in hypoxia

Both in mice that had been 6h and 24h in hypoxia, we found expression of a set of DEX responsive genes that were not induced by DEX in normoxia. It concerns 61 genes at 6h and 50 genes at 24h (**Fig 2B, D**), showing an overlap of only 6 genes. An overview of these genes can be found in **Dataset EV1** (6h) and **Dataset EV2** (24h). Examples are shown in **Fig 3A** and **3B**. The number of these newly acquired DEX-responsive genes is considerably less compared to the amount of DEX responsive genes that are lost by hypoxia (262 genes at 6h, 294 genes at 24h). The general expression pattern of these genes was also evaluated in normoxia and hypoxia alone. Boxplots were used based on the median of the LFCs of these genes after 6h and 24h hypoxia (**Appendix Figure S2A, B**). First, when comparing the LFCs directly in normoxia and hypoxia, a median LFC of around 0 is observed. This indicates that hypoxia alone does not have an influence on the expression level of these genes. Second, DEX stimulation in normoxia does not lead to a significant induction of these genes but shows a fairly large non-significant fold change. The individual LFC values tend towards a lower expression in hypoxia compared to normoxia. Overall, when hypoxia is combined with DEX treatment, DEX counteracts the initial downregulation that is observed in hypoxia alone. In hypoxia, the DEX effect is enhanced indicating that both hypoxia and DEX stimulation are necessary to induce the expression of this subset of genes. Since these genes are expressed by GR in hypoxic conditions, a crosstalk between GR and HIF may form the mechanism of this induction. By studying the pathways induced by the union of these DEX-induced genes in hypoxia via Enrichr, we found that peroxisome proliferator-activated receptor alpha (PPAR α) is the top-activated transcription factor. Also GR and HIFs were found. When analysing pathways that are induced by these unique DEX responsive genes in hypoxia, Enrichr revealed exclusively metabolic pathways, including fatty acid β -oxidation. Finally, the top GO associated biological response found via Enrichr, was the response to GCs. Together, these data suggest that in hypoxia DEX is sensed, GR, PPAR α , HIF1 α and HIF2 α are activated, and metabolic reprogramming is induced.

We then studied the GR DNA-binding profile of these specific DEX responsive genes in hypoxia. A clear DEX effect in hypoxia was observed when plotting the LFC of these genes induced by DEX in hypoxic conditions compared to the expression of these genes after DEX in normoxia (**Fig 3C**). Based on the GR DNA-binding sites associated with DEX responsive genes in hypoxia, an increase in the coverage of these GR DNA-binding peaks was observed after DEX in hypoxia compared to PBS (**Fig 3D**). However, the increase in peak coverage was still lower after DEX stimulation in hypoxia

compared to normoxia, indicating that other mechanisms could be involved next to the alterations in the GR DNA-binding profile responsible for the differences that we observed in the transcriptomics data. The GR DNA-binding peaks of *Slc22a5* 6h and 24h after hypoxia and DEX stimulation are shown in **Fig 3E**. Using HOMER *de novo* motif search, we could not detect a clear link between GR and HIF which could be responsible for the induction of the DEX responsive genes in hypoxia alone. We also investigated the expression levels of *Slc25a30* in the liver of HIF1 α HIF2 α ^{fl/fl} and HIF1 α HIF2 α ^{AlbKO} mice after 6h hypoxia stimulated or not with DEX. The absence of HIF1 α and HIF2 α in the liver did not alter the expression pattern of *Slc25a30* (**Fig 3F**). In conclusion, we identified DEX responsive genes in hypoxia linked with metabolic pathways and higher GR DNA-binding after DEX stimulation in hypoxia. Further investigation will be necessary to identify other mechanisms involved in the regulation of the expression of these specific DEX responsive genes in hypoxia.

Hypoxia causes activation of GR by HPA axis stimulation

Since we have shown that the response to DEX under hypoxia is less pronounced, we wanted to investigate whether the GR is already activated upon exposure to hypoxia and therefore GR is not able to respond to DEX. Based on the RNA-seq data, we found that hypoxia induced the expression of typical GR responsive genes in the liver (LFC > 1 and P < 0.05): 51 genes after 6h hypoxia (**Fig 4A**) and 99 genes after 24h hypoxia (**Fig 4B**), with 26 genes overlapping. These genes are known GR-stimulated genes, as they were also induced by DEX in normoxia in the RNA-seq data, so these genes will be referred to as 'stress GRE genes'. A heatmap of these stress GRE genes is displayed in **Fig 4C**. **Fig EV2** shows heatmaps of the GR responsive genes after 6h (**Fig EV2A**) and 24h (**Fig EV2B**) of hypoxia. A functional survey via Enrichr of the union of the 6h and 24h genes (124 genes) reveals that transcription factors such as GR, PPAR α and HIFs, but also c-Myc, Nanog, Smad3, are associated with the expression of these genes. We studied whether the induction of these stress GRE genes in hypoxia can be linked with an increase in GR DNA-binding. The coverage of GR DNA-binding peaks was clearly higher after DEX stimulation in normoxia (**Fig EV3A, B**) but, when comparing the peak coverage in normoxia and hypoxia only, we observed an increase in GR DNA-binding peaks in hypoxia for both time points, although less obvious after 24h. The GR DNA-binding peaks for *Cdkn1a* (**Fig EV3C**), *Mfsd2a* (**Fig EV3D**), *Ddit4* (**Fig EV3E**) and *Igfbp1* (**Fig EV3F**) are shown as examples.

To investigate whether the induction of the stress GRE genes during hypoxia in the liver can be attributed to the activation of the HPA axis, we validated the RNA-seq data via RT-qPCR in C57BL/6J and ADX mice, of which both adrenal glands are surgically removed. The expression levels of *Cdkn1a*, *Mfsd2a*, and *Ddit4* were significantly increased in hypoxic conditions in C57BL/6J mice, both after 6h (**Fig 4D**) and 24h (**Fig 4E**), but not in ADX mice (**Fig 4D, E**) and the plasma GC levels were significantly

higher after 6h and 24h of hypoxia in C57BL/6J mice (**Fig 4F, G**). Since hypoxia increases GC production by the adrenal glands, we considered if hypoxia leads to the activation of the entire HPA axis by studying *Crh* mRNA levels in the hypothalamus and plasma ACTH levels during hypoxia. Indeed, both *Crh* (**Fig 4H**) and ACTH (**Fig 4I**) showed a transient increase. Also, plasma GC levels were significantly elevated after hypoxia (**Fig 4J**). To rule out whether the caging of the mice has an influence on the GC production, C57BL/6J mice were housed in normal cages and in a normoxic chamber and blood was collected after 2h, 6h and 24. No differences in GC levels were observed (**Appendix Fig S3**). Furthermore, we also investigated the hypothalamic response in ADX mice in hypoxia. Hypothalamic *Crh* mRNA levels were increased after 2h hypoxia in C57BL/6J mice. It is known that *Crh* mRNA levels are higher in ADX mice (Dallman *et al*, 1994) because of a lack of GC control. Similar *Crh* mRNA levels were observed in the hypothalamus of C57BL/6J and ADX mice in hypoxia (**Fig EV3G**), however due to high basal *Crh* mRNA levels in ADX mice, no significant difference was detected in ADX mice. The expression level of stress GRE genes was also measured in the hypothalamus of C57BL/6J and ADX mice after 2h hypoxia. A significant increase was observed after 2h hypoxia in C57BL/6J mice, however these levels were significantly reduced in the hypothalamus of ADX mice (**Fig EV3H**). To confirm that the GC levels were reduced in ADX mice, GC levels were measured in the plasma of these mice. In C57BL/6J mice, GC levels were significantly increased in hypoxia (2h), while this was not the case in ADX mice (**Fig EV3I**). Based on these data, it is likely that hypoxia activates the entire HPA axis, starting with *Crh* transcription in the hypothalamus, leading to ACTH and the induction of stress GRE genes in a GC dependent way.

Since ADX mice fail to activate GR, it could be possible that the reduced GC production also has an effect on HIF activity in general, as was shown in GR deficient zebrafish *larvae* (Marchi *et al*, 2020). Therefore, we have investigated the expression pattern of HIF target genes in the liver of C57BL/6J and ADX mice in normoxia and hypoxia (6h and 24h). Fold inductions (H/N) were calculated between C57BL/6J and ADX mice for these genes. The mean fold induction in C57BL/6J mice was generally around 1.6, indicating an increase in the expression of HIF target genes in hypoxia. However, a significant reduction of the fold induction (1.2) in ADX mice was observed (**Fig EV2C**), suggesting that the absence of GC production influences the expression of HIF target genes. The expression pattern of a number of HIF target genes is shown in **Fig EV2D**. A future study is necessary to further investigate the impact of GR on HIF function.

GR is critical during the hypoxia induced stress response

We further investigated the role of GR in the stress response during hypoxia (6h) by inhibiting GR using RU486, and by using GR^{dim/dim} mice, which express a GR with a reduced dimerization potential

and therefore are unable to induce dimer-dependent GRE genes. RU486 pre-treated mice (**Fig 4K**) and GR^{dim/dim} mice (**Fig 4L**) were no longer able to increase the expression of hypoxia induced stress GRE genes in the liver. We further investigated whether the presence of HIF1 α and HIF2 α in the liver is essential for the expression of these stress GRE genes. Both in HIF1 α HIF2 α ^{AlbKO} mice and wild-type littermates, *Cdkn1a*, *Mfsd2a* (**Fig 4M**), *Ddit4* and *Igf1* (**Appendix Fig S4A**) were significantly upregulated 6h after hypoxia, suggesting that the induction of the stress GRE genes depend exclusively on GCs and GR. As a proof of concept, the expression of HIF target genes was also studied in the liver of HIF1 α HIF2 α ^{fl/fl} and HIF1 α HIF2 α ^{AlbKO} mice in hypoxia (6h) and was significantly reduced upon hypoxic conditions in the absence of liver HIF1 α and HIF2 α (**Appendix Fig S4B**).

Finally, we examined the response of ADX mice to DEX regarding genes induced by DEX in normoxia but not in hypoxia in C57BL/6J mice (**Fig 2**, for example *Hspa1a*). In hypoxic conditions (24h), when ADX mice were stimulated with DEX, typical GRE genes like *Hspa1a* were significantly upregulated both in normoxia and hypoxia. Also, unique DEX responsive genes induced by hypoxia (**Fig 3**) were expressed in ADX mice (**Fig 4N**). Based on these results, we conclude that the chronic GC production by the adrenals in hypoxia is responsible for the altered DEX response in the liver of hypoxic mice and is independent of liver HIF1 α and HIF2 α .

Involvement of hypothalamic HIF1 α and HIF2 α in activation of the HPA axis

To investigate the influence of hypoxia on gene expression in the hypothalamus we performed an RNA-seq analysis 2h after hypoxia and found significant increase of 313 genes at the level of the hypothalamus (LFC > 0.3 and P < 0.05). HOMER motif enrichment analysis based on known motifs (vertebrates) identified 80 genes containing an HIF1 β motif in their promoter (**Fig 5A**), also the HIF1 α and HIF2 α motif (**Fig 5B**) as well as the GRE motif were found. Based on the expression levels of the stress GRE genes and the appearance of HREs in the HOMER analysis it is obvious that the hypothalamus reacts on HIF transcription factors as well as on the GR to hypoxia. Enrichr Pathway analysis coupled the 313 upregulated genes to a HIF signalling response but it also showed that the transcription factor Hey2, which is a HIF1 α /HIF2 α induced gene, is associated with the observed differential expression in the hypothalamus. Hey2 binds the E-box motif CACGTG (Steidl *et al*, 2000), the same motif which is bound by other transcription factors such as NPAS, NPAS2, c-Myc, CLOCK, BMAL and others, all of which were retrieved via HOMER motif enrichment analysis. The expression of stress GRE genes at the level of the hypothalamus was validated using RT-qPCR (**Fig 5C**). In addition, western blot as well as immunohistochemistry (IHC) confirmed HIF1 α and HIF2 α protein stability in hypothalamus 2h after hypoxia (**Fig 5D**). In normoxia, HIF1 α and HIF2 α were mainly found in the cytoplasm, while a clear nuclear enrichment was observed during hypoxia (**Fig 5E**). In

conclusion, hypoxia stimulates the HPA axis, leading to GC production and the induction of stress GRE genes in liver and hypothalamus. Additionally, both HIF1 α and HIF2 α are stabilized and clear enrichment in the nuclei of hypothalamic cells during hypoxia was detected.

Hypoxia causes lipolysis and liver ketogenesis in a GR-dependent manner

The transcriptomics data in the liver and Enrichr pathway analyses suggest that hypoxia instruct GR to regulate metabolic rather than inflammatory pathways. PPAR α (encoded by the *Nr1c1* gene) is one of the major sensors of the nutritional status and it is highly expressed in the liver and primarily controls the oxidation of FFAs and ketogenesis (Wang *et al*, 2020; Grabacka *et al*, 2016). We investigated the metabolic profile of mice under hypoxic conditions and the effect on liver PPAR α activity. The plasma of C57BL/6J and ADX mice was collected 6h after normoxia or hypoxia for metabolic profile analysis. In the plasma of C57BL/6J control mice, the levels of numerous different FFAs were significantly increased after 6h of hypoxia, while no differences were detected in the plasma of ADX mice (**Fig 6A**). **Fig 6B** depicts several examples. A complete overview of the metabolic profile is shown in **Fig EV4A**. Since FFAs are endogenous ligands and activators of PPAR α , we investigated the PPAR α gene response to hypoxia by measuring PPAR α responsive genes (*Ppara* itself and *Hmgcs2*) in the liver. During early hypoxia (6h), no significant changes were observed (**Fig EV4B**) but the PPAR α response was significantly increased after 24h hypoxia (**Fig 6C**). To support that hepatic PPAR α is activated, the expression level of PPAR α dependent genes was measured via RT-qPCR in liver-specific PPAR α knock-out (PPAR α^{AlbKO}) mice. The expression of these genes was significantly upregulated after 24h in wild-type mice, while the expression levels were significantly reduced in the liver of PPAR α^{AlbKO} mice upon hypoxia (**Fig EV4C**). To exclude whether DEX itself is able to induce the expression of *Ppara* and PPAR α responsive genes (*Cd36*, *Cpt1a*, *Cpt2*, *Slc25a20*, *Hadha*, *Acat1*, *Acox1*, *Acox2*, *Ehhadh* and *Hmgcs2*) in normoxia and hypoxia (6h and 24h), we calculated the fold inductions (DEX/PBS) of these genes (**Fig EV4D**). We were unable to detect significant differences between the fold inductions in normoxia and hypoxia. Since the fold inductions are mainly around 1, we can assume that DEX is not sufficient to induce *Ppara* and PPAR α responsive genes.

We further examined the role of GR in the release of FFAs in the plasma of mice during hypoxia. Inhibition of GR by RU486 prevented the release of FFAs in the plasma (**Fig 6D**) while in GR^{dim/dim} mice, FFA levels were still increased by hypoxia, suggesting that the increased FFA production in white adipose tissue (WAT) is not affected by the reduced dimerization potential of GR^{dim/dim} mice (**Fig 6E**). FFA levels were also measured in the plasma of PPAR α^{AlbKO} mice and wild-type littermates after 6h hypoxia. In basal conditions, the FFA levels were already significantly higher in the plasma of PPAR α^{AlbKO} mice. These results are in line with the increased hepatic and plasma FFA levels in full

PPAR α knock-out mice (Kersten *et al*, 1999; Leone *et al*, 1999). As expected, hypoxia significantly increased FFA levels in PPAR α ^{fl/fl} mice. However, no difference could be observed in PPAR α ^{AlbKO} mice due to the high basal levels (**Fig EV4E**). Since the WAT is the most essential organ for lipolysis (Bolsoni-Lopes & Alonso-Vale, 2015), and GR can activate lipolysis (de Guia & Herzig, 2015), we studied if the stress GRE response is induced by hypoxia (6h) in inguinal WAT (iWAT) and whether this response is GR dependent. Both in mice pre-treated with RU486 (**Fig 6F**) and GR^{dim/dim} mice (**Fig 6G**), the expression of stress GRE genes was absent during hypoxia.

Because the expression of *Hmgcs2*, the rate-limiting enzyme in the ketone body (KB) biosynthesis (McGarry & Foster, 1980), is significantly increased after 24h of hypoxia, we investigated the effect of hypoxia on the production of KBs. Three endogenous KBs, namely β -hydroxybutyrate (BHB), acetoacetate and acetone, are produced via ketogenesis in the liver, starting from acetyl-CoA (Van Wyngene *et al*, 2018). The metabolomics analysis showed a significant increase of BHB in the plasma of C57BL/6J mice 6h after hypoxia, but not in ADX mice (**Fig 6H**). Acetoacetic acid also tended to increase upon hypoxia, while these levels were lower in ADX mice (**Fig EV4F**). The last KB acetone was not detected via the metabolomics analysis. Furthermore, to investigate whether a reduced food intake might be responsible for the differences in KB production between C57BL/6J and ADX mice, the average food intake of C57BL/6J and ADX mice after 24h normoxia or hypoxia was determined. We did not observe a difference in food intake between C57BL/6J and ADX mice in normoxia and hypoxia, however a significant reduction in food intake was observed in both C57BL/6J and ADX mice during hypoxic conditions (**Fig EV4G**). When GR was inhibited via RU486, KBs were not elevated in the plasma of these mice (**Fig 6I**). Interestingly the increase in KBs was absent in GR^{dim/dim} mice (**Fig 6J**), suggesting that intact GR dimerization is a necessary companion of PPAR α (as shown earlier in starvation studies (Ratman *et al*, 2016)) for ketogenesis in hypoxia. We also confirmed the involvement of PPAR α in the KB production, since KB levels were significantly increased in PPAR α ^{fl/fl} mice, while this was absent in PPAR α ^{AlbKO} mice (**Fig EV4H**). To support that FFA production in hypoxia, is due to lipolysis, we investigated the weight of iWAT in C57BL/6J and ADX mice and found significant decrease in C57BL/6J mice while in ADX mice, although their iWAT weight was already lower compared to C57BL/6J control mice, no effect was observed (**Fig 6K**). In conclusion, hypoxia leads to the activation of the HPA axis, which activates GR in the liver, hypothalamus and iWAT. In the latter, hypoxia has GR dimer regulated stress effects as well as lipolytic effects, causing FFA release, and hepatic PPAR α activation and KB production.

GR shows attenuated anti-inflammatory capacity under hypoxic conditions

As we have demonstrated that liver GR is less responsive to DEX in hypoxia (**Fig 2**) and hypoxia activates the HPA axis, leading to higher GC production (**Fig 4**), we studied if hypoxia attenuates the anti-inflammatory actions of DEX and if DEX is still able to protect against LPS-induced lethal endotoxic shock (**Fig 7, Fig EV5**). *Nfkb1a*, *Dusp1* and others such as *Fam107a*, *Tsc22d3*, *Vdr* and *Serpina3c* were significantly upregulated by DEX in normoxia, however less induced by DEX in hypoxia. Also, genes with known pro-inflammatory capacities are repressed by DEX in normoxia, but are repressed to lesser extent by DEX in hypoxia (**Fig EV5**). These effects are most pronounced in the liver 24h after hypoxia (**Fig EV5B**) and are less clear after 6h (**Fig EV5A**). We measured the expression levels of *Dusp1* and *Nfkb1a* via RT-qPCR and found that they can no longer be induced by DEX 24h after hypoxia in the liver, lung, kidney and spleen (**Fig 7A**). We then studied whether DEX-induced protection against LPS-induced endotoxemia (Dejager *et al*, 2010; Kleiman *et al*, 2012), a very well-known acute lethal inflammation model, is different in hypoxia compared to normoxia. First, we compared the LPS sensitivity of mice kept for 24h in hypoxia or normoxia by increasing the dose of i.p. injected LPS (2.5 mg/kg, 5 mg/kg and 14.5 mg/kg LPS) and recording lethal response. Mice in hypoxia displayed a higher sensitivity to LPS (**Fig 7B**). In order to confirm that the LD₁₀₀ LPS dose in normoxia and hypoxia is comparable in terms of organ damage, parameters (lactate dehydrogenase (LDH), aspartate transaminase (AST), creatine kinase, urea) were measured in the plasma of mice 6h after LPS injection. The increase of LDH, AST, creatine kinase and urea was similar in the plasma of mice in normoxia and hypoxia in LPS-induced endotoxemia (**Fig 7C**). It is known that LPS causes fast activation of the HPA axis leading to increased GC levels and repression of the pro-inflammatory response of LPS (Beishuizen & Thijs, 2003). Since hypoxia induces chronic GC production, and since we hypothesize that the anti-inflammatory function of GCs is compromised, GC levels were measured in the plasma of mice in normoxia and hypoxia 2h after LPS injection. In normoxia, LPS causes a significant increase in GC levels while in mice in hypoxia, no further increase could be observed when LPS is injected (**Fig 7D**). Next, the effect of LPS on the expression of genes with a known anti-inflammatory function was measured via RT-qPCR and these genes (*Fam107a*, *Dusp1*, *Tsc22d3*, *Vdr* and *Serpina3c*) were significantly induced after LPS injection in normoxia, but no difference in gene expression was detected in hypoxic conditions (**Fig 7E**). Furthermore, the expression of these genes was significantly increased in ADX mice by DEX stimulation (**Fig 7F**) in normoxia as well as in hypoxia, indicating that the chronic GC production, via the activation of the HPA axis by hypoxia, might be responsible for a reduced anti-inflammatory induction by LPS or by injection of DEX.

C57BL/6J mice were treated with DEX (10 mg/kg) or PBS after 24h normoxia or hypoxia, followed 1h later by a single lethal LPS dose (normoxia 14.5 mg/kg LPS, hypoxia 5 mg/kg LPS). In normoxia, DEX

was found to protect mice against LPS-induced lethality, while no DEX protection was observed in mice under hypoxic conditions (**Fig 7G**). Also, a clear DEX effect was detected on organ damage parameters 24h after LPS injection in normoxia (**Fig EV5D**), but not in hypoxia (**Fig EV5E**). It is known that GCs are important in preserving glucose levels during inflammatory conditions such as sepsis, since glucose is the primary energy source of the brain and it is important to maintain the maximal brain function upon inflammation (Kuo *et al*, 2015; Van Wyngene *et al*, 2018; Vandewalle & Libert, 2020). Based on our results, hypoxia activates the HPA axis thereby increasing GC levels, which are not further increased upon an inflammatory stimulus such as LPS (**Fig 7D**). To investigate whether the activation of the HPA axis and increased GC levels in hypoxia have an influence on the glucose levels during inflammation, we performed an experiment in which female C57BL/6J mice were put in normoxia or hypoxia for 24h followed by an intraperitoneal injection with PBS or DEX (10 mg/kg). 1h later, these mice were injected intraperitoneally with 14.5 mg/kg LPS (normoxia) or 5 mg/kg (hypoxia). As expected, blood glucose levels were decreased 24h after LPS-induced endotoxemia in normoxia, DEX was not able to increase this (**Fig EV5F**). Similar results were obtained when mice were in hypoxic conditions (**Fig EV5G**), thereby indicating that the activation of the HPA axis and increased GC levels do not alter the glucose response to inflammation. To confirm that chronic GC production is responsible for the lack of DEX protection in hypoxia, we investigated whether DEX remained able to protect against a lethal LPS dose (0.05 mg/kg LPS) in ADX mice in hypoxia. First, LD₁₀₀ LPS was checked in ADX mice both in normoxia and hypoxia. No difference in LPS sensitivity could be observed (**Fig EV5C**). In ADX mice, DEX was still able to induce a significant protection against a lethal LPS dose, independent of the O₂ concentration in which the ADX mice were kept (**Fig 7H**). In conclusion, the anti-inflammatory function of DEX is compromised under hypoxic conditions. **The activation of the HPA axis followed by a chronic GC production by hypoxia might be responsible for this compromised function of DEX.**

Discussion

The cellular responses to stress and inflammation are tightly regulated by the GC-induced and hypoxia-induced transcriptional responses. Several *in vitro* and *in vivo* studies using zebrafish *larvae* have illustrated the presence of a crosstalk between HIF and GR (Vanderhaeghen *et al*, 2021; Vettori *et al*, 2017; Marchi *et al*, 2020). Although these papers are very valuable, more convincing data is necessary to understand the impact of hypoxia on GR in a pathophysiological context *in vivo*. Therefore, we have investigated the *in vivo* impact of hypoxia on GR function in mice by genome-wide transcriptional analysis in liver and by means of deep hypoxia. During these experiments mice have been put under extreme hypoxic conditions [we applied 7% O₂ based on previous studies (Bruder *et al*, 2008; Wang *et al*, 2012b)], however no mortality was detected after 6h or 24h hypoxia. Hypoxia stabilizes hypothalamic HIF1 α and HIF2 α and causes a complete, strong activation of the HPA axis and chronic production of GCs by the adrenals. As it is difficult to obtain blood from mice in a non-stressed manner (Kim *et al*, 2018), the GC levels observed in normoxia might be potentially stress levels. In the absence of GC production via adrenalectomy, the negative feedback signal is removed thereby increasing CRH and ACTH levels (Dallman *et al*, 1987, 1994). The importance of the HPA axis activation and GC production regarding the stress GRE response was confirmed in ADX mice upon hypoxia. As expected, basal *Crh* mRNA levels were increased in ADX mice, hypoxia tended to increase the *Crh* mRNA levels in ADX mice although not significant and to similar extent as C57BL/6J mice. The effect of reduced GC production was also clear on the expression levels of the stress GRE genes. In GR deficient zebrafish *larvae*, the reduced GC production also affects HIF activity in general (Marchi *et al*, 2020). We have observed a significant reduction in the fold induction of HIF target gene expression levels in ADX mice upon hypoxia, suggesting that GCs also influences the expression of HIF target genes. Further research is needed to determine the details of the contribution of HIF1 α and/or HIF2 α in the activation of the HPA axis upon hypoxia and the GC/GR stress response, and how GC/GR regulate these HIF effects.

Since the activation of the HPA axis is an essential component of how GR is engaged to a more metabolic program during hypoxia, we have studied this in more detail. Our data suggest that hypoxia (i) activates several GRE genes by means of HPA axis activation and GC production, (ii) causes DEX to induce genes that are not induced by DEX in normoxia in which hypoxia and DEX exert a synergistic effect, and (iii) strongly reduces the effect of DEX on canonical DEX-induced genes in the liver. Based on RT-qPCR analysis in ADX mice, this last effect appears to be due to the HPA axis activation, although we do not have RNA-seq data of ADX mice in normoxia and hypoxia combined with DEX stimulation. Furthermore, the effects of hypoxia on the gene expression patterns are

independent on the presence of HIF1 α and HIF2 α in the liver. The mechanisms of action of GCs include binding of GC to the cytoplasmic GR, GR translocation to the nucleus, followed by DNA binding and regulation of gene expression (Timmermans *et al*, 2019). In our study, we found that hypoxia had no significant effects on *Nr3c1* mRNA levels. Although it has been shown that increased GC levels can reduce GR protein levels, a phenomenon called homologous downregulation (Dong *et al*, 1988; Bellingham *et al*, 1992), liver GR protein levels were not decreased in hypoxic conditions. GR homologous downregulation is proposed as one of the mechanisms causing GCR (Van Bogaert *et al*, 2011; Dendoncker *et al*, 2019), however GR is still active in hypoxic conditions, but its priorities are clearly altered. The reprogramming of GR induced during hypoxia is, in part, regulated by differences in the GR DNA-binding profiles. Based on ChIP-seq analysis, we found that (i) the induction of stress GRE genes by hypoxia can be linked with increases in GR DNA-binding, (ii) the DEX responsive genes in hypoxia which are not induced by DEX in normoxia are associated with a higher coverage of GR DNA-binding peaks after DEX in hypoxia compared to PBS, however the overall peak coverage is still lower in comparison to DEX stimulation in normoxia, and (iii) the strongly reduced DEX effect on canonical DEX-induced genes by hypoxia can be correlated with reduced GR DNA-binding after DEX stimulation in the liver. We were not able to find evidence for a direct interaction between GR and HIF, which is in line with the results of Yang *et al*. They also found that hypoxia depletes GR target genes involved in inflammatory responses and that hypoxia increases the expression of genes involved in O₂ regulation (Yang *et al*, 2020), which we can confirm based on our RNA-seq data. Alterations in GR DNA-binding are thus partly responsible for the changes in DEX response in hypoxia.

Next to alterations in the GR DNA-binding profiles, hypoxia can also induce changes in the chromatin structure via histone methylation, acetylation and DNA methylation (Batie *et al*, 2018). Histone acetylation is correlated with transcriptional activation, independent of the acetylation site. Acetylation of histone H3 on lysine 27 (H3K27ac) is the most studied histone acetylation and is known as a marker for active enhancers (Calo & Wysocka, 2013). Recently, Yang *et al*. (2020) have identified a differential acetylation of H3K27 in response to DEX in hypoxia. These changes in GR activation chromatin state might also be responsible for changes in the GR recruitment to DNA (Yang *et al*, 2020). The p300 co-activator is also known as a powerful mediator of GR transactivation and brings histone acetylation enzymatic activity to the GR bound sites (Guo *et al*, 2017; Dendoncker *et al*, 2019). More than half of the GR DNA-binding site have shown enrichment of the p300 co-activator and thus an active histone mark (Yang *et al*, 2020), indicating that competition between GR and HIF for the p300 co-activator might also be responsible for the alterations in the gene expression profile. Finally, hypoxia drives the expression of both miRNA 103 and 107, which causes a decreased

expression of its known target KLF4 followed by the inhibition of GR co-modulators such as CARM1, NCOA2 (Chen *et al*, 2012; Yang *et al*, 2020). Further investigation will be necessary to determine whether posttranslational modifications such as histone acetylation contribute to the GR response during hypoxic conditions and/or whether the induction of miRNAs are involved in the altered GR DNA-binding and transcriptomics profile upon hypoxia.

As mentioned, endogenous GCs promote lipolysis under a normal, basal physiologic state via the induction of lipase activity in the adipose tissue of mice (de Guia & Herzig, 2015). The mode of action of GR is thought to be (i) via gene induction of the Angiotensin Like 4 gene (*Angptl4*) (ii) as well as by inhibition of the phosphodiesterase 3 gene (*Enpp3* gene), both leading to increased phosphorylation and activation of hormone sensitive lipase by PKA, but also via (iii) increased gene expression of the Adipose Tissue Triacylglycerol lipase-coding gene (*Pnpla2*) (Wang *et al*, 2012a). In hypoxia, the production of GCs is dependent on the adrenals, since GC levels are significantly lower in the plasma of ADX mice. Of note, an important remark in the use of ADX mice is the fact that not only GCs, but also catecholamines like epinephrine and norepinephrine are no longer produced by the adrenal medulla (Kanczkowski *et al*, 2016). Since hypoxia-induced FFA release is also blocked by RU486, it is clear, however, that this hypoxia effect is a GR effect and not a catecholamine response. The fact that GR^{dim/dim} mice still respond to hypoxia by increased FFA levels argues for a requirement of intact GR dimerization in this regard in WAT. The stress GRE response is also induced in the iWAT and is intact GR dimerization-dependent, showing that the GR reprogramming is also present in this tissue.

In Peruvian populations living at high altitude, a unique dyslipidemia pattern with high frequency of triglyceride levels have been observed (Gonzales & Tapia, 2013). Since FFAs are endogenous ligands of PPAR α (Wang *et al*, 2020), the effect of hypoxia on β -oxidation was further investigated. We reveal that hypoxia increases plasma FFA levels and PPAR α -mediated β -oxidation followed by enhanced KB production (ketogenesis). Upon fasting, PPAR α full knock-out mice fail to induce mitochondrial and peroxisomal fatty acid oxidation genes (Lee & Gonzalez, 1996), which leads to increased levels of plasma and hepatic fatty acids, hypoketonemia and hypothermia (Leone *et al*, 1999; Kersten *et al*, 1999). In PPAR α ^{AlbKO} mice, plasma FFA levels were higher during basal conditions. Although we expected an increase of FFAs upon hypoxia in PPAR α ^{AlbKO} mice, no significant differences were observed in the plasma of these mice. This might be associated with an increased fatty acid uptake and lipid accumulation in the liver (Kersten *et al*, 1999; Yasuhara *et al*, 1991). Since the production of KBs is also dependent on intact GR dimerization, a close interaction between GR and PPAR α during ketogenesis in hypoxia appears essential. GR-PPAR α physical interaction during ketogenesis in starvation has already been shown *in vitro* by Ratman *et al*. (Ratman *et al*, 2016). Furthermore, PPAR α agonists are able to inhibit the expression of GC-responsive GRE-driven genes in a PPAR α

dependent manner (Bougarne *et al*, 2009). Also, the anti-inflammatory activity of DEX is lower in PPAR α knock-out mice compared to wild-type littermates (Cuzzocrea *et al*, 2008), corroborating the crosstalk between PPAR α and GR. We also evaluated whether DEX itself is sufficient to induce PPAR α mediated fatty acid oxidation pathways. However, no effect of DEX on the expression levels of genes involved in β -oxidation was detected.

Several studies have investigated the function of HIF1 α and HIF2 α in lipid metabolism. Although we did not observe an increase in lipid biosynthesis, Li *et al*. showed that HIF1 α upregulates lipid biosynthesis in the liver by stimulating sterol regulatory element binding protein (SREBP)-1 activity via SREBP cleavage-activating protein (SCAP) during intermittent hypoxia (Li *et al*, 2006). However, a protective role for HIF1 α in the development of alcoholic fatty liver is proven by Nishiyama *et al*. The absence of HIF1 α in the liver leads to increased lipid biosynthesis and steatosis (Nishiyama *et al*, 2012). Although we observed an increase in β -oxidation during hypoxia, Liu *et al*. found that inhibition of the HIF1 α or HIF2 α in the liver attenuates hypoxia-reduced FFA β -oxidation leading to improved hepatic fat metabolism. However, a dominant role for HIF1 α in the decrease in β -oxidation is stated by Belanger *et al*. (Belanger *et al*, 2007), while Rankin *et al*. suggest an important role for HIF2 α in attenuating β -oxidation (Rankin *et al*, 2009). We also detected higher KB levels in hypoxia and their dependency on the intact GR dimerization. The absence of HIF1 β in mouse livers leads to decreased KB levels, suggesting a role for HIF1 α and/or HIF2 α in ketogenesis (Wang *et al*, 2009). Further investigation will be necessary to uncover the exact role of HIF1 α and/or HIF2 α and their link with PPAR α in lipid metabolism and ketogenesis during hypoxia.

Hypoxia and inflammation are two closely linked phenomena in many pathological processes such as critical illness, sepsis and inflammatory bowel diseases (IBDs). Critically ill patients often experience systemic inflammation in combination with hypoxia. Kiers *et al*. (2018) found that mice, exposed to 9% O₂ 1h before systemic inflammation, display an attenuated inflammatory cytokine response (Kiers *et al*, 2018). This is in contrast with the results obtained in our study where prolonged hypoxia (24h, 7% O₂) causes an increased sensitivity to a lethal LPS-induced endotoxemia. Hypoxia is also present in tumours and is recognized as an important deleterious factor in cancer therapies. In tumours, enhanced angiogenesis is present, however O₂ levels are significantly lower ranging from 0.3 – 4.2% O₂ (McKeown, 2014). In acute inflammation under normal O₂ concentrations, when mice are injected with tumour necrosis factor (TNF) or LPS, endogenous GCs are important protective molecules against this SIRS (De Bosscher *et al*, 2016). They are well known for their anti-inflammatory properties, primarily by counteracting the production of pro-inflammatory cytokines, such as IL-1 β , IL-6, and IFN β (De Bosscher *et al*, 2003; Libert *et al*, 1990, 1991). Adrenalectomy causes a clear sensitization of mice to acute lethal SIRS induced by LPS (Dejager *et al*, 2010), illustrating that LPS

causes HPA axis activation and GC production (Beishuizen & Thijs, 2003), thereby inducing the expression of genes with anti-inflammatory functions in a negative feedback mechanism. We found that the LPS sensitivity in ADX mice is not altered in the presence of low O₂ concentrations, and DEX can still protect these mice. The chronic GC production by hypoxia is thus responsible for the increased sensitivity for LPS and for the lack of DEX protection, since genes with anti-inflammatory functions can no longer be upregulated by LPS, because no additional GCs can be induced. Previously, we have shown that in acute, lethal inflammation like septic shock, a functional decline of GR is observed, called GCR (Van Bogaert *et al*, 2011; Dendoncker *et al*, 2019). Despite GR is still functional in a condition of pure, deep hypoxia, it seems that the anti-inflammatory priority of GR has changed to a more metabolic function. Since GR DNA-binding is required for its anti-inflammatory function (Escoter-Torres *et al*, 2020; Uhlenhaut *et al*, 2013), the altered DEX response and the changes in the anti-inflammatory profile of GR in hypoxia could be correlated with the differences in the GR DNA-binding profile after DEX stimulation, when mice are in hypoxic conditions. The use of GCs attenuates the pro- and anti-inflammatory responses present during sepsis. The first large scale clinical trials considering the use of GCs in sepsis patients involved high doses of GCs in the management of septic shock. Bolus injection of GCs significantly reduced the mortality rates (Minneci *et al*, 2009). However, more recent clinical trials recommend the use of a supraphysiological dose of hydrocortisone (200-300 mg/day)(Annane *et al*, 2002). In contrast to the supraphysiological dose of GCs, we used a rather high dose of DEX (10 mg/kg) because this concentration protects prophylactically against a lethal LPS-induced endotoxemia (Van Looveren *et al*, 2020) and we wanted to investigate the effect of hypoxia on the pro- and anti-inflammatory functioning of the GR. However, we have to take into account that other nuclear receptors such as the pregnane X receptor (PXR) might also be activated when using such a high dose of DEX (Pavek, 2016).

Since inflammation is able to induce the stabilization and activation of HIF (Cummins *et al*, 2016), it would be of great interest to know whether HIF might play a role in the GCR during sepsis. The protective effects of exogenous GCs like DEX against LPS-induced endotoxemia are frequently associated with the inhibition of TNF production in white blood cells, such as macrophages (Bhattacharyya *et al*, 2007; Kleiman *et al*, 2012; Van Looveren *et al*, 2020). Nevertheless, hepatic GR is also crucial for the GC homeostasis and the protection against SIRS and sepsis (Van Bogaert *et al*, 2011; Jenniskens *et al*, 2018). When ascending to high altitude, factors like immunomodulation, hypoxia, environmental stressors and physiologic adaptations may lead to increased susceptibility to pathogens (Basnyat & Starling, 2015). The most common syndrome starting within a few hours of ascent is acute mountain sickness (AMS). It is generally associated with headache, nausea, vomiting, anorexia, lassitude and sleep disturbances (Taylor, 2011). Several studies have shown that

prophylactic treatment of humans with synthetic GCs like DEX (Rock *et al*, 1989; Basu *et al*, 2002a; Kitsteiner *et al*, 2011), prednisolone (Basu *et al*, 2002b) or budesonide (Berger *et al*, 2017; Zhu *et al*, 2020; Zheng *et al*, 2014) prevent the development of AMS or reduce its symptoms. In contrast, our study shows that a few hours after hypoxia, the anti-inflammatory GR response to DEX is strongly reduced compared to normoxia, probably due to the change in more metabolic priorities of the GR. We could speculate that DEX will first influence the metabolic functions of GR during hypoxia, while the anti-inflammatory functions are less important. When people are pre-treated with an exogenous GC like DEX before ascending to high altitude, the main anti-inflammatory function of GR is not altered and will be able to prevent the development of AMS. In this regard, the actual outcome of the interplay between GR and hypoxia may depend on a 'first come' principle. However, it would be of great interest to identify the effect of less severe hypoxia on the GR function, if the GC/GR response would be different. Also adaptation to long-term hypoxia could alter the metabolic and inflammatory effects linked to GR we observe during acute, deep hypoxia.

In summary, hypoxia activates the HPA axis, leading to GC production by the adrenal glands. The precise role of HIF1 α and/or HIF2 α in this activation requires further investigation. GCs are responsible for increased lipolysis and FFA levels in the bloodstream independent of intact GR dimerization. FFAs induce PPAR α activity in the liver, leading to the production of KBs, which is GR dimerization-dependent. Next to GR-mediated metabolic changes, hypoxia sensitizes mice to LPS-induced endotoxemia which is caused by the HPA axis activation and GC production. Furthermore, DEX is no longer able to protect mice against LPS-induced lethal shock and is probably linked with the changes in the GR DNA-binding profile in hypoxia. Our data unfold new physiological pathways that may have consequences for patients suffering from GCR, when ascending to high altitudes or when hypoxia is present in critically ill patients.

Materials and Methods

Mice. Female C57BL/6J mice as well as bilaterally adrenalectomized (ADX) C57BL/6J mice were purchased from Janvier (Le Genest-St. Isle, France). ADX mice were ordered at the age of 7 weeks and bilateral adrenalectomy was performed two weeks before delivery. $HIF1\alpha^{fl/fl}$, $HIF2\alpha^{fl/fl}$ (provided by Dr. Ben Wielockx) and $PPAR\alpha^{fl/fl}$ (provided by Prof. Dr. Karolien De Bosscher) were crossed with *Albumin Cre* transgenic mice, and the offspring was intercrossed to generate $HIF1\alpha^{fl/fl} Albumin Cre^{Tg/+}$ ($HIF1\alpha^{AlbKO}$), $HIF2\alpha^{fl/fl} Albumin Cre^{Tg/+}$ ($HIF2\alpha^{AlbKO}$), $HIF1\alpha HIF2\alpha^{fl/fl} Albumin Cre^{Tg/+}$ ($HIF1\alpha HIF2\alpha^{AlbKO}$) and $PPAR\alpha^{fl/fl} Albumin Cre^{Tg/+}$ ($PPAR\alpha^{AlbKO}$) mice, all in a C57BL/6J background. $GR^{dim/dim}$ mice were generated by Reichardt *et al.* (1998) (Reichardt *et al.*, 1998) and kept on a FVB/N background (generously provided by Dr. Jan Tuckermann, Ulm, Germany). Heterozygous $GR^{dim/wt}$ mice were intercrossed to generate $GR^{wt/wt}$ and $GR^{dim/dim}$ homozygous mutant mice. All offspring was genotyped by PCR on genomic DNA isolated from toe biopsies. Mice were housed in a temperature-controlled, specific pathogen free (SPF) air-conditioned animal house with 14 and 10h light/dark cycles and received food and water *ad libitum*. The drinking water of ADX mice was supplemented with 0.9% NaCl. All mice were used at the age of 8 – 12 weeks, and all experiments were approved by the institutional ethics committee for animal welfare of the Faculty of Sciences, Ghent University, Belgium.

Reagents. LPS from *Salmonella abortus equi* was purchased from Sigma-Aldrich N.V. (L-5886). For *in vivo* DEX injection, Rapidexon (Medini N.V.) was used. LPS and DEX were diluted in pyrogen-free phosphate buffered saline (PBS). RU486 (Mifepristone, Sigma-Aldrich N.V.), a GR antagonist, was diluted in DMSO. Luciferin (XenoLight™ D-Luciferin - K+ Salt) was purchased from Caliper Life Sciences.

Injections and sampling. All injections were given intraperitoneally (i.p.), except for the hydrodynamic intravenous (i.v.) tail injection of the DNA plasmid. Injection volumes were always adapted to the bodyweight of the mice. In lethality experiments, mice were monitored by monitoring rectal body temperature. Mice with body temperature below 28°C were euthanized using cervical dislocation. Blood was taken via cardiac puncture after sedation of the mice with a ketamine/xylazine solution (Sigma-Aldrich N.V.) or via retro-orbital eye bleeding after sedation with isoflurane. To obtain mouse plasma, samples blood was collected in EDTA-coated tubes, and samples were centrifuged at 3,000 rpm for 15 minutes at 4°C. Plasma samples were stored at -80°C for metabolomics analysis or at -20°C for biochemical analysis. For sampling of liver and white adipose tissue, mice were killed by cervical dislocation at indicated time points.

Hypoxia treatment. Mice were randomly assigned to the normoxia group and hypoxia group. The normoxia group was exposed to room air (21% O₂), whereas the hypoxia group was placed in a ventilated hypoxic chamber with 7% O₂ and 93% N₂ for the indicated time points. The oxygen levels were monitored with a Greisinger GOX 100 oxygen sensor (Conrad).

Detection of HIF activity. Mice were injected in the tail vein over five seconds with a HRE-luciferase reporter plasmid solution (Addgene, #26731; 10 µg/ml in sterile, endotoxin-free PBS) or PBS (control) in a volume equivalent to 10% of the body weight, as described by Van Bogaert *et al.* (2011) (Van Bogaert *et al.*, 2011). The HRE-luciferase plasmid contains three hypoxia response elements (24-mers, TGTCACGTCCTGCACGACTCTAGT) from the *Pgk1* gene upstream of firefly luciferase. Five hours after transfection (HRE-Luc 0h), mice were placed in normoxic or hypoxic conditions, and visualized after indicated time points. Briefly, mice were injected with 200 µl of a 15 mg/ml potassium salt luciferin solution. 10 minutes after injection, livers were isolated and visualized via the imaging chamber of the IVIS Spectrum *In Vivo* Imaging System (Caliper Life Sciences). Photon emission was integrated over a period of 2 minutes and recorded as pseudo-colour images. Living Image (Caliper Life Sciences) was used for image analysis. The regions of interest (ROI, red circles) were selected based on the luciferase signal (purple) detected over all images. To confirm the specificity of the technique used for the injection of the HRE-luciferase reporter plasmid, liver and other organs were also visualised (**Fig 1B**; PBS, HRE-Luc N, HRE-Luc H 1h, HRE-Luc H 2h). For the PBS injected mice and mice injected with the HRE-luciferase plasmid in normoxia, only 1 picture is shown representing the luciferase signal at the different time points when mice were put in normoxia or hypoxia. Data were acquired as photons/cm²/s and results are normalized to the PBS control group. N = normoxia, H = hypoxia.

Food intake experiment. To determine whether hypoxia has an influence on the food intake during hypoxia, C57BL/6J or ADX mice were placed in normoxia or hypoxia for 24h with access to a limited amount of food. The food was weighed at the start of the experiment, and 2h, 6h and 24h after the start of the experiment. Alternating experiments were performed with C57BL/6J and ADX mice in normoxia and hypoxia with 4-5 mice per group. The amount of food eaten during the experiment was calculated and divided by the amount of mice present per group to calculate the average amount of food (in grams) each mouse had eaten over 24h. The experiment with C57BL/6J or ADX mice was performed in triplicate.

RNA sequencing.

Liver

Total RNA was isolated with Aurum total RNA mini kit (Biorad) according to the manufacturer's instructions. RNA concentration was measured, and RNA quality was checked with the Agilent RNA 6000 Pico Kit (Agilent Technologies). The 6h library was constructed using the TruSeq Stranded mRNA Library Prep kit (Illumina) according to the manufacturer's instructions and sequenced paired-end on an Illumina NextSeq500 instrument. The 24h library was constructed using a Stranded NextSeq high output mRNA Library Prep kit (2x150p) according to the manufacturer's instructions and sequenced single-end on an Illumina NextSeq500 instrument. The data were quality checked and pre-processed (Illumina adapter removal) with Trimmomatic v 0.39 (Bolger *et al*, 2014). Reads were mapped to the mouse (mm10) reference genome using known splice junctions from the Ensemble 95 version of the annotation with HISAT2 (Kim *et al*, 2019). Gene level reads counts were obtained with featureCounts (Liao *et al*, 2014) and differential expressed genes were found by the DESeq2 R package (Love *et al*, 2014) with the false discovery rate (FDR) set at 5%. Motif finding for multiple motifs or *de novo* motif finding was performed using the HOMER software. We used the promoter region (start offset: -1 kb, end offset: 50 bp downstream of transcription start site (TSS)) to search for known motif enrichment and *de novo* motifs (Heinz *et al*, 2010). Visualizations were made using the R software. Gene ontology (GO) term enrichment on selected gene groups was performed via the Enrichr tool (Chen *et al*, 2013).

Hypothalamus

Total RNA was isolated with Aurum total RNA mini kit (Biorad) according to the manufacturer's instructions. RNA concentration was measured, and RNA quality was checked with the Agilent RNA 6000 Pico Kit (Agilent Technologies). The 2h library was constructed using the TruSeq Stranded mRNA Library Prep kit (Illumina) according to the manufacturer's instructions and sequenced paired-end on an Illumina NextSeq500 instrument. The data were quality checked and pre-processed (Illumina adapter removal) with Trimmomatic v 0.39 (Bolger *et al*, 2014). Reads were mapped to the mouse (mm10) reference genome using known splice junctions from the Ensemble 95 version of the annotation with HISAT2 (Kim *et al*, 2019). Gene level reads counts were obtained with featureCounts (Liao *et al*, 2014) and differential expressed genes were found by the DESeq2 R package (Love *et al*, 2014) with the false discovery rate (FDR) set at 5%. Motif finding for multiple motifs or *de novo* motif finding was performed using the HOMER software. We used the promoter region (start offset: -1 kb, end offset: 50 bp downstream of TSS) to search for known motif enrichment and *de novo* motifs (Heinz *et al*, 2010). Visualizations were made using the R software. Gene ontology (GO) term enrichment on selected gene groups was performed via the Enrichr tool (Chen *et al*, 2013).

Real-time quantitative PCR. Liver was isolated and stored in RNA later (Life Technologies Europe), and white adipose tissue was snap frozen and stored at -20°C before RNA was isolated. Total RNA

was isolated with the Aurum total RNA mini kit (Biorad) according to manufacturer's instructions. RNA concentration was measured with the Nanodrop 8000 (Thermo Fisher Scientific), and 1000 ng RNA was used to prepare cDNA with Sensifast cDNA Synthesis Kit (Bioline). cDNA was diluted 20 times in ultrapure water for use in RT-PCR reactions. RT-PCR primers for used targets are listed in Table 2. RT-PCR reaction was performed with sensiFast Sybr no-ROX mix (Bioline) and was performed in duplicate in a Roche LightCycler480 system (Applied Biosystems). The stability of the housekeeping genes (HKGs) were determined by Genorm. Results are given as relative expression values normalized to the geometric mean of the HKGs, calculated in the qBase+ software (Biogazelle).

Metabolomics experiments. Plasma metabolites were extracted by adding 10 μ L of plasma to 990 μ L of an 80% methanol (in water) extraction buffer containing 2 μ M of deuterated (d27) myristic acid as internal standard). Following extraction overnight at -80°C . Precipitated proteins and insolubilities were removed by centrifugation at 20.000 x g for 20 minutes at 4°C . The supernatant was transferred to the appropriate mass spectrometer vials. Measurements were performed using a Vanquish LC System (Thermo Scientific) in-line connected to a Lumos Orbitrap mass spectrometer (Thermo Scientific). 2 μ l of sample was injected and concentrated on a Hilicon iHILIC-Fusion(P) SS precolumn after which it was loaded onto a Hilicon iHILIC-Fusion(P) SS column SS (Achrom). A linear gradient was carried out starting with 90% solvent A (LC-MS grade acetonitrile) and 10% solvent B (10 mM ammoniumacetate pH 9.3). From 2 to 20 minutes the gradient changed to 80% B and was kept at 80% until 23 minutes. Next a decrease to 40% B was carried out to 25 minutes, further decreasing to 10% B at 27 minutes. Finally, 10% B was maintained until 35 minutes. The solvent was used at a flow rate of 200 μ l/min, the columns temperature was kept constant at 25°C . The mass spectrometer operated in negative ion mode, settings of the HESI probe were as follows: sheath gas flow rate at 35, auxiliary gas flow rate at 14. Spray voltage was set at 2.9 kV, temperature of the capillary at 300°C and S-lens RF level at 50. A full scan (resolution of 240.000 and scan range of m/z 70-750) was applied. For the data analysis, we used Compound Discoverer 3.0 (Thermo Scientific) a software platform for analysing metabolites. Identification of metabolites was done with in-house libraries as well as with third party databases.

Endotoxemia experiments. 24h before LPS injections, mice were put under normoxic or hypoxic conditions for 24h. Female C57BL/6J mice were injected i.p. with PBS or DEX (10 mg/kg) followed by a lethal dose of LPS (LD_{100} 14.5 mg/kg in normoxia, 5 mg/kg in hypoxia) dissolved in sterile PBS to induce endotoxin shock. Female ADX mice were injected i.p. with a lethal LPS dose of 0.05 mg/kg. For survival experiments, rectal body temperature and lethality were monitored. For experiments aimed to isolate blood and organ samples, mice were injected i.p. with LPS or PBS in control mice. For

biochemical analysis, mice were euthanized via cervical dislocation at indicated time points and plasma and organs were isolated.

Biochemical analysis. Analysis of mouse plasma aspartate aminotransferase (AST), alanine aminotransferase (ALT), creatinine, troponin, creatine kinase (CK) and lactate dehydrogenase (LDH) levels were kindly provided to us by the University Hospital of Ghent. Blood glucose and ketone body levels were measured in tail blood with the use of OneTouch Verio glucose meter (LifeScan) and Freestyle Precision Neo meter (Abbott), respectively. ACTH (Antibodies-online GmbH), corticosterone (Tebu-Bio) and free fatty acid (Abnova) were measured in mouse plasma with the use of colorimetric assays according to manufacturer's instructions.

Western blot analysis.

Liver

For the detection of GR, total protein was isolated out of snap frozen liver with RIPA lysis buffer, supplemented with protease inhibitor cocktail (Roche). Protein samples containing 50 µg of protein was separated by electrophoresis on a 8% gradient SDS-polyacrylamide gel and transferred to nitrocellulose filters (pore size 0,45 µm). After blocking the membranes with a ½ dilution of Starting Block/PBST 0.1% (Thermo Fisher Scientific), membranes were incubated overnight at 4°C with primary antibodies against GR α/β (1:1000, G5, sc-393232; Santa Cruz,) and β -actin (1:5000; Life Technologies Europe) as an internal control. Blots were washed with PBST 0.1% and then incubated for 1h at room temperature with Amersham ECL anti-mouse antibody (1:2000, NA931, GE Healthcare Life Sciences). Immunoreactive bands were visualized and quantified using an Amersham Imager 600 (GE Healthcare Life Sciences).

Hypothalamus

For western blot, hypothalamus tissue samples were lysed for protein extraction using RIPA buffer with inhibitors: PMSF, protease inhibitors, sodium orthovanadate (all from Chem cruz). The tissue samples were lysed under hypoxic conditions (3% O₂) in the whitley hypoxia chamber. For lysis, samples were incubated for 30 minutes on ice and with periodic vortexing followed by centrifugation for removal of debris. The samples were aliquoted and then stored at -80°C until further processing. The protein concentrations were measured using the Bicinchoninic acid assay (BCA) (Thermo Fischer). 25 µg of protein from each sample was mixed with LDS sample buffer and 5% mercaptoethanol and denaturation was performed at 99°C for 5 minutes. Following denaturation, proteins were separated on a 4-12% Bis-Tris protein gels (Thermo Fisher) and transferred to the membrane. The membranes were blocked with 5% Milk with TBST. After washing, the membranes

were incubated with primary antibodies overnight at 4°C. The primary antibodies used were: HIF-1 α (Cayman chemical) or HIF-2 α (Abcam), or later with Vinculin (Cell signalling) after stripping in 5% Milk with TBST. After overnight incubation with primary antibodies, the membranes were washed followed by incubated with secondary Rabbit IgG HRP (R&D systems) for 1h at room temperatures. The membranes were then subjected to imaging using Fusion Fx (Peqlab, VWR). The quantifications were performed using Fiji (ImageJ distribution 1.52K).

Immunohistochemistry.

Liver

For the evaluation of the transfection efficiency of the HRE-luciferase reporter plasmid, excised liver from PBS and HRE-Luc injected mice were fixed in 4% paraformaldehyde overnight at 4°C, dehydrated and embedded in paraffin. Tissue sections of 5 μ m were cut. For the luciferase staining, tissue sections were dewaxed, incubated with antigen retrieval buffer (1x citrate buffer pH6, Vector H-3300) for 20 min at boiling temperature in a PickCell electric pressure cooker and cooled down. Peroxidase blocking was done with 3% H₂O₂ in methanol for 10 min. Blocking buffer (5% goat serum in 1% bovine serum albumin (BSA) in PBS) was added to the slides for 30 min at room temperature. Primary antibody against luciferase (MA1-16880, ThermoFisher Scientific) was diluted 1:1000 in 1% BSA in PBS and incubated overnight at 4°C. Then, slides were incubated with the goat anti-mouse secondary HRP antibody (MP-7452, Vector Laboratories, 1:5 in PBS) for 30 min. To signal of the staining was increased via incubating the slides with the Tyramide Signal Amplification (TSA) kit (1:75, Perkin Elmer) for 10 min, followed by 30 min incubation with ABC (PK-6100, Vector Laboratories). Counterstaining was done with Hoechst reagent (Sigma-Aldrich NV, 1:1000 in PBS). Pictures were taken with an Olympus BX51 Discussion Microscope.

Hypothalamus

For immunofluorescence staining of HIF1 α and HIF2 α on hypothalamus samples, OCT embedded hypothalamus tissue was cut into 7 μ m sections at -20°C using a cryotome and stored at -20°C until further processing. For staining, the sections were dried for 20 minutes at room temperature. Fixed with para-formaldehyde, washed with phosphate-buffered saline (PBS), and with PBS containing 0.1% Tween-20, blocked with 5% normal goat serum followed by primary antibody staining with HIF1 α (Cayman chemical) or HIF2 α (Novus biologicals) for 3 days at 4°C and subsequent secondary antibody staining. Slides were mounted in fluorescent mounting medium and stored at 4°C until analysis. Fluorescent images were acquired on an ApoTome II Colibri (Carl Zeiss, Jena, Germany), scale bar (50 μ m). Images were analysed using either Zen software (Carl Zeiss, Jena, Germany) or Fiji (ImageJ distribution 1.52K).

ChIP-sequencing. ChIP-seq was used to investigate the GR DNA-binding in conditions of normoxia and hypoxia using biological triplicates for all conditions, for a total of 18 analysed samples (3 N_PBS, 3 N_DEX, 3 H_PBS_6h, 3 H_DEX_6h, 3 H_PBS_24h and 3 H_DEX_24h) and input controls. All conditions were processed in one run, which included the immunoprecipitation (IP) and sequencing. Therefore, all comparisons listed in the manuscript are considered “within experiment” comparisons. Snap frozen liver samples were derived from mice that were injected with PBS or 10 mg/kg DEX in normoxic conditions and 6h or 24h after hypoxia. 200 mg of tissue was homogenized in PBS and then crosslinked with 2% formaldehyde in PBS for 20 minutes at RT while rotating. This reaction was stopped by adding 125 mM glycine for 10 minutes at RT. Tissue was then collected in ice-cold PBS and subsequently lysed in lysis buffer (0.1% SDS, 1% Triton X-100, 0.15 M NaCl, 1 mM EDTA and 20 mM Tris pH8, supplemented with protease inhibitors). Lysates were sonicated at 4°C to yield 200-800 bp DNA fragments. IP was performed on 100 µl lysates diluted 1:3 in incubation buffer (0.15% SDS, 1% Triton X-100, 0.15 M NaCl, 1 mM EDTA and 20 mM HEPES) with 5 µg of rabbit anti-GR antibody (H300, sc-8992; Santa Cruz) or normal rabbit IgG (10500C; Invitrogen) as negative control at 4°C overnight. After 2h BSA blocked nProtein sepharose beads (GE Healthcare) were added to the lysates. The following day, beads were washed in WBI, WBII, LiCl buffer and twice in EDTA/HEPES buffer (0.5 M EDTA and 1 M HEPES). Chromatin was eluted in 200 µl elution buffer (0.1 M NaHCO₃ and 10% SDS) supplemented with proteinase K. Next, proteins were decrosslinked by raising the incubation temperature to 65°C for 16h and DNA purified using the PCR purification kit (Qiagen), and eluting in 50 µl of Qiagen Elution Buffer. Fifteen ng of purified DNA was used to generate ChIP-seq libraries according to manufacturer’s protocol using NEBNext Ultra II DNA Library Prep Kit (E7645L, NEB). Libraries were single-end sequencing by Illumina NextSeq 500. The ChIP-seq experiment was performed in collaboration with the group of Jorma J. Palvimo (Finland), where the IP pulldown, library preparation and sequencing were executed. Spike-in samples were not used based on their experience and the fact that all samples were processed within one experiment. Samples were normalized for sequencing depth, background signal and scaled to 1e7 reads per sample per condition. These scaled data were used for all visualisations. The obtained reads were mapped to the mm10 reference genome using the bwa software (bwa mem). Peak calling was done using HOMER v4.11 (Heinz *et al*, 2010) requiring 4-fold enrichment over input and local background and at least 50 tags per peak. To increase our data reliability and counter variability, only bound regions found in all 3 replicates of a condition were considered in this work. Motif finding, annotation, visualisations and detection of differentially bound regions was also done with HOMER (find motifs genome, annotate peaks and find differential peak replicates). Peak region motif finding was done 1 kb upstream to 50 bp downstream of the TSS.

Statistics. Data were expressed as means \pm standard errors of the means (SEM). Statistical significance was evaluated with two-way unpaired Student's t-test and one-way or two-way ANOVA in GraphPad Prism 8.0 software (GraphPad Software, San Diego, CA). If applicable, one-way and two-way ANOVA analysis were followed by post-hoc analysis to correct for multiple testing during the pairwise multiple comparisons using the Tukey's test or the Šídák's multiple comparisons test for one-way and two-way ANOVA, respectively. **The results of the two-way ANOVA tests can be found in Dataset EV3.** Fold changes or ratios were log (Y) transformed before statistical analysis. Survival curves were subjected to the Log-Rank (Mantel-Cox) test to investigate whether statistical significance could be observed during different groups. The Pearson correlation coefficient (PCC) was determined using the R statistics software and the correlation coefficient function.

Data availability. RNA-seq data: Gene expression. Deposited at the National Center for Biotechnology Information Gene Expression Omnibus public database (<http://www.ncbi.nlm.nih.gov/geo/>) under accession numbers GSE162100 and GSE162155 for RNA-seq data 6h and 24h after hypoxia and DEX stimulation in liver, respectively, accession number GSE162673 for RNA-seq data of hypothalamus samples (2h hypoxia). CHIP-seq data: accession number GSE163242.

Acknowledgements

The authors wish to thank Jan Tuckermann, Ben Wielockx and Karolien De Bosscher for providing GR^{dim/dim} mice, HIF1a^{fl/fl} and HIF2a^{fl/fl} mice, and PPARa^{fl/fl} mice respectively. We thank Joke Vanden Berghe and animal house caretakers for animal care. We acknowledge the VIB Nucleomics Core for RNA sequencing. The EMBL GeneCore is acknowledged for CHIP sequencing. Research in the author's laboratories was funded by the Agency for Innovation of Science and Technology in Flanders (IWT), the Research Council of Ghent University (GOA grant BOF19-GOA-004 and Methusalem grant BOF.MET.2021.0001.0), the Research Foundation Flanders (FWO-Vlaanderen Research grants G025220N and G014921N and SBO-grant S002721N and S003122N) and Flanders Institute for Biotechnology (VIB).

Author contributions

Contributions: T.V. conceived and performed the experiments and co-wrote the manuscript. S.T. performed all bio-informatics analysis of RNA sequencing and CHIP sequencing data. L.V.W, K.V.L., J.V., C.W., L.D., G.C., K.D.B. and L.N. performed experiments. M.E., S.D., J.D.B. and J.V.B. provided general technical assistance. W.V.B. provided a hypoxia chamber and performed part of the hypoxia experiments. B.G. did the metabolomics experiments. B.W. and D.W. did Western Blot analysis and immunohistochemistry for HIF1a and HIF2a on hypothalamus samples. K.L. performed the immunohistochemistry for luciferase on the liver samples. J.P. and V.P. performed the processing of the samples for CHIP sequencing. R.B. and C.L. supervised the research and co-wrote the manuscript.

Conflict of interest

The authors have no conflicts of interest or financial interests associated with this paper.

References

- Annane D, Sébille V, Charpentier C, Bollaert PE, François B, Korach JM, Capellier G, Cohen Y, Azoulay E, Troché G, *et al* (2002) Effect of treatment with low doses of hydrocortisone and fludrocortisone on mortality in patients with septic shock. *J Am Med Assoc* 288: 862–871
- Basnyat B & Starling JM (2015) Infectious Diseases at High Altitude. *Microbiol Spectr* 3: 1–7
- Basu M, Sawhney RC, Kumar S, Pal K, Prasad R & Selvamurthy W (2002a) Glucocorticoids as prophylaxis against acute mountain sickness. *Clin Endocrinol (Oxf)* 57: 761–767
- Basu M, Sawhney RC, Kumar S, Pal K, Prasad R & Selvamurthy W (2002b) Hypothalamic-pituitary-adrenal axis following glucocorticoid prophylaxis against acute mountain sickness. *Horm Metab Res* 34: 318–324
- Batie M, del Peso L & Rocha S (2018) Hypoxia and chromatin: A focus on transcriptional repression mechanisms. *Biomedicines* 6: 1–19
- Bauer A, Tronche F, Wessely O, Kellendonk C, Reichardt HM, Steinlein P, Schütz G & Beug H (1999) The glucocorticoid receptor is required for stress erythropoiesis. *Genes Dev* 13: 2996–3002
- Beishuizen A & Thijs LG (2003) Endotoxin and the hypothalamo-pituitary-adrenal (HPA) axis. *J Endotoxin Res* 9: 3–24
- Belanger AJ, Luo Z, Vincent KA, Akita GY, Cheng SH, Gregory RJ & Jiang C (2007) Hypoxia-inducible factor 1 mediates hypoxia-induced cardiomyocyte lipid accumulation by reducing the DNA binding activity of peroxisome proliferator-activated receptor α /retinoid X receptor. *Biochem Biophys Res Commun* 364: 567–572
- Bellingham DL, Sar M & Cidlowski JA (1992) Ligand-dependent down-regulation of stably transfected human glucocorticoid receptors is associated with the loss of functional glucocorticoid responsiveness. *Mol Endocrinol* 6: 2090–2102
- Berger MM, Macholz F, Sareban M, Schmidt P, Fried S, Dankl D, Niebauer J, Bärtsch P & Mairbörl H (2017) Inhaled budesonide does not prevent acute mountain sickness after rapid ascent to 4559 m. *Eur Respir J* 50: 1–4
- Bhattacharyya S, Brown DE, Brewer JA, Vogt SK & Muglia LJ (2007) Macrophage glucocorticoid receptors regulate Toll-like receptor 4-mediated inflammatory responses by selective inhibition of p38 MAP kinase. *Blood* 109: 4313–4319

- Bleymehl K, Pérez-Gómez A, Omura M, Moreno-Pérez A, Macías D, Bai Z, Johnson RS, Leinders-Zufall T, Zufall F & Mombaerts P (2016) A Sensor for Low Environmental Oxygen in the Mouse Main Olfactory Epithelium. *Neuron* 92: 1196–1203
- Van Bogaert T, Vandevyver S, Dejager L, Van Hauwermeiren F, Pinheiro I, Petta I, Engblom D, Kleyman A, Schütz G, Tuckermann J, *et al* (2011) Tumor necrosis factor inhibits glucocorticoid receptor function in mice: A strong signal toward lethal shock. *J Biol Chem* 286: 26555–26567
- Bolger AM, Lohse M & Usadel B (2014) Trimmomatic: A flexible trimmer for Illumina sequence data. *Bioinformatics* 30: 2114–2120
- Bolsoni-Lopes A & Alonso-Vale MIC (2015) Lipolysis and lipases in white adipose tissue – An update. *Arch Endocrinol Metab* 59: 335–342
- De Bosscher K, Beck IM, Ratman D, Berghe W Vanden & Libert C (2016) Activation of the Glucocorticoid Receptor in Acute Inflammation: The SEDIGRAM Concept. *Trends Pharmacol Sci* 37: 4–16
- De Bosscher K, Vanden Berghe W & Haegeman G (2003) The interplay between the glucocorticoid receptor and nuclear factor- κ B or activator protein-1: Molecular mechanisms for gene repression. *Endocr Rev* 24: 488–522
- Bougarne N, Paumelle R, Caron S, Hennuyer N, Mansouri R, Gervois P, Staels B, Haegeman G & De Bosscher K (2009) PPAR α blocks glucocorticoid receptor α -mediated transactivation but cooperates with the activated glucocorticoid receptor α for transrepression on NF- κ B. *Proc Natl Acad Sci U S A* 106: 7397–7402
- Bruder ED, Taylor JK, Kamer KJ & Raff H (2008) Development of the ACTH and corticosterone response to acute hypoxia in the neonatal rat. *Am J Physiol Regul Integr Comp Physiol* 295: 1195–1203
- Calo E & Wysocka J (2013) Modification of Enhancer Chromatin: What, How, and Why? *Mol Cell* 49: 825–837
- Chang AJ, Ortega FE, Riegler J, Madison D V. & Krasnow MA (2015) Oxygen regulation of breathing through an olfactory receptor activated by lactate. *Nature* 527: 240–244
- Chen EY, Tan CM, Kou Y, Duan Q, Wang Z, Meirelles GV, Clark NR & Ma'ayan A (2013) Enrichr: interactive and collaborative HTML5 gene list enrichment analysis tool. *BMC Bioinformatics* 14: 1–14

- Chen HY, Lin YM, Chung HC, Lang YD, Lin CJ, Huang J, Wang WC, Lin FM, Chen Z, Huang H Da, *et al* (2012) MiR-103/107 promote metastasis of colorectal cancer by targeting the metastasis suppressors DAPK and KLF4. *Cancer Res* 72: 3631–3641
- Cockman ME, Masson N, Mole DR, Jaakkola P, Chang G, Clifford SC, Maher ER, Pugh CW, Ratcliffe PJ & Maxwell PH (2000) Hypoxia Inducible Factor- α Binding and Ubiquitylation by the von Hippel-Lindau Tumor Suppressor Protein *. *J Biol Chem* 275: 25733–25741
- Cummins EP, Keogh CE, Crean D & Taylor CT (2016) The role of HIF in immunity and inflammation. *Mol Aspects Med*: 24–34 doi:10.1016/j.mam.2015.12.004 [PREPRINT]
- Cuzzocrea S, Bruscoli S, Mazzon E, Crisafulli C, Donato V, Di Paola R, Velardi E, Esposito E, Nocentini G & Riccardi C (2008) Peroxisome proliferator-activated receptor- α contributes to the anti-inflammatory activity of glucocorticoids. *Mol Pharmacol* 73: 323–337
- Dallman MF, Akana SF, Jacobson L, Levin N, Cascio CS & Shinsako J (1987) Characterization of Corticosterone Feedback Regulation of ACTH Secretion. *Ann N Y Acad Sci* 512: 402–414
- Dallman MF, Akana SF, Levin N, Walker CD, Bradbury MJ, Suemaru S & Scribner KS (1994) Corticosteroids and the control of function in, the hypothalamo-pituitary-adrenal (HPA) axis. *Ann N Y Acad Sci* 746: 22–31
- Daniel Bird A, McDougall ARA, Seow B, Hooper SB & Cole TJ (2015) Minireview: Glucocorticoid regulation of lung development: Lessons learned from conditional GR knockout mice. *Mol Endocrinol* 29: 158–171
- Dejager L, Pinheiro I, Puimège L, Fan YD, Gremeaux L, Vankelecom H & Libert C (2010) Increased glucocorticoid receptor expression and activity mediate the LPS resistance of SPRET/EI mice. *J Biol Chem* 285: 31073–31086
- Dendoncker K, Timmermans S, Vandewalle J, Eggermont M, Lempiäinen J, Van Hamme E, Dewaele S, Vandevyver S, Ballegeer M, Souffriau J, *et al* (2019) TNF- α inhibits glucocorticoid receptor-induced gene expression by reshaping the GR nuclear cofactor profile. *Proc Natl Acad Sci U S A* 116
- Dong Y, Poellinger L, Gustafsson JÅ & Okret S (1988) Regulation of glucocorticoid receptor expression: Evidence for transcriptional and posttranslational mechanisms. *Mol Endocrinol* 2: 1256–1264
- Escoter-Torres L, Greulich F, Quagliarini F, Wierer M & Uhlenhaut NH (2020) Anti-inflammatory functions of the glucocorticoid receptor require DNA binding. *Nucleic Acids Res* 48: 8393–8407

- Franke K, Gassmann M & Wielockx B (2013) Erythrocytosis: The HIF pathway in control. *Blood* 122: 1122–1128
- Garcia-alvarez M, Marik P & Bellomo R (2014) Sepsis-associated hyperlactatemia. *Crit Care* 18: 1–11
- Gonzales GF & Tapia V (2013) Association of high altitude-induced hypoxemia to lipid profile and glycemia in men and women living at 4100m in the Peruvian Central Andes. *Endocrinol y Nutr (English Ed)* 60: 79–86
- Grabacka M, Pierzchalska M, Dean M & Reiss K (2016) Regulation of ketone body metabolism and the role of PPAR α . *Int J Mol Sci* 17
- de Guia RM & Herzig S (2015) How do glucocorticoids regulate lipid metabolism? *Adv Exp Med Biol* 872: 127–144
- Guo B, Huang X, Cooper S & Broxmeyer HE (2017) Glucocorticoid hormone-induced chromatin remodeling enhances human hematopoietic stem cell homing and engraftment. *Nat Med* 23: 424–428
- Harrell CS, Rowson SA & Neigh GN (2015) Pharmacological stimulation of hypoxia inducible factor-1 α facilitates the corticosterone response to a mild acute stressor. *Neurosci Lett* 600: 75–79
- Heinz S, Benner C, Spann N, Bertolino E, Lin YC, Laslo P, Cheng JX, Murre C, Singh H & Glass CK (2010) Simple Combinations of Lineage-Determining Transcription Factors Prime cis-Regulatory Elements Required for Macrophage and B Cell Identities. *Mol Cell* 38: 576–589
- Jenniskens M, Weckx R, Dufour T, Perre S Vander, Pauwels L, Derde S, Téblick A, Güiza F, Van Den Berghe G & Langouche L (2018) The hepatic glucocorticoid receptor is crucial for cortisol homeostasis and sepsis survival in humans and Male mice. *Endocrinology* 159: 2790–2802
- Jungermann K & Kietzmann T (2000) Oxygen: Modulator of metabolic zonation and disease of the liver. *Hepatology* 31: 255–260
- Kanczkowski W, Sue M & Bornstein SR (2016) Adrenal gland microenvironment and its involvement in the regulation of stress-induced hormone secretion during sepsis. *Front Endocrinol (Lausanne)* 7: 1–9
- Kersten S, Seydoux J, Peters JM, Gonzalez FJ, Desvergne B & Wahli W (1999) Peroxisome proliferator-activated receptor alpha mediates the adaptive response to fasting. *J Clin Invest* 103: 1489–1498
- Kiers D, Wielockx B, Peters E, van Eijk LT, Gerretsen J, John A, Janssen E, Groeneveld R, Peters M,

- Damen L, *et al* (2018) Short-Term Hypoxia Dampens Inflammation in vivo via Enhanced Adenosine Release and Adenosine 2B Receptor Stimulation. *EBioMedicine* 33: 144–156
- Kim D, Paggi JM, Park C, Bennett C & Salzberg SL (2019) Graph-based genome alignment and genotyping with HISAT2 and HISAT-genotype. *Nat Biotechnol* 37: 907–915
- Kim S, Foong D, Cooper MS, Seibel MJ & Zhou H (2018) Comparison of blood sampling methods for plasma corticosterone measurements in mice associated with minimal stress-related artefacts. *Steroids* 135: 69–72
- Kitsteiner JM, Whitworth JD & Nashelsky J (2011) Preventing acute mountain sickness. *Am Fam Physician* 84: 398–400
- Kleiman A, Hubner S, Rodriguez Parkitna JM, Neumann A, Hofer S, Weigand MA, Bauer M, Schmid W, Schutz G, Libert C, *et al* (2012) Glucocorticoid receptor dimerization is required for survival in septic shock via suppression of interleukin-1 in macrophages. *FASEB J* 26: 722–729
- Kodama T, Shimizu N, Yoshikawa N, Makino Y, Ouchida R, Okamoto K, Hisada T, Nakamura H, Morimoto C & Tanaka H (2003) Role of the Glucocorticoid Receptor for Regulation of Hypoxia-dependent Gene Expression *. *J Biol Chem* 278: 33384–33391
- Kuo T, McQueen A, Chen T-C & Wang J-C (2015) Regulation of Glucose Homeostasis by Glucocorticoids. *Adv Exp Med Biol* 872: 99–126
- Lee SST & Gonzalez FJ (1996) Targeted Disruption of the Peroxisome Proliferator-Activated Receptor alpha Gene, PPARalpha. *Ann N Y Acad Sci* 804: 524–529
- Leonard MO, Godson C, Brady HR & Taylor CT (2005) Potentiation of Glucocorticoid Activity in Hypoxia through Induction of the Glucocorticoid Receptor. *J Immunol* 174: 2250–2257
- Leone TC, Weinheimer CJ & Kelly DP (1999) A critical role for the peroxisome proliferator-activated receptor α (PPAR α) in the cellular fasting response: The PPAR α -null mouse as a model of fatty acid oxidation disorders. *Proc Natl Acad Sci U S A* 96: 7473–7478
- Li J, Bosch-Marce M, Nanayakkara A, Savransky V, Fried SK, Semenza GL & Polotsky VY (2006) Altered metabolic responses to intermittent hypoxia in mice with partial deficiency of hypoxia-inducible factor-1 α . *Physiol Genomics* 25: 450–457
- Liao Y, Smyth GK & Shi W (2014) FeatureCounts: An efficient general purpose program for assigning sequence reads to genomic features. *Bioinformatics* 30: 923–930
- Libert C, Bladel S Van, Brouckaert P, Shaw A, Fiers W, Libert C, Bladel VAN, Brouckaert P & Shaw A

- (1991) Involvement of the liver , but not of IL-6 , in IL-1-induced desensitization to the lethal effects of tumor necrosis factor . This information is current as Why The JI ? Submit online . • Rapid Reviews ! 30 days * from submission to initial decision • No. *J Immunol* 146: 2625–2632
- Libert C, Brouckaert P, Shaw A & Fiers W (1990) Induction of interleukin 6 by human and murine recombinant interleukin 1 in mice. *Eur J Immunol* 20: 691–694
- Van Looveren K, Timmermans S, Vanderhaeghen T, Wallaey C, Ballegeer M, Souffriau J, Eggermont M, Vandewalle J, Wyngene L Van, Bosscher K De, *et al* (2020) Glucocorticoids limit lipopolysaccharide-induced lethal inflammation by a double control system. *EMBO Rep* 32: 1–17
- Love MI, Huber W & Anders S (2014) Moderated estimation of fold change and dispersion for RNA-seq data with DESeq2. *Genome Biol* 15: 1–21
- Marchi D, Santhakumar K, Markham E, Li N, Storbeck KH, Krone N, Cunliffe VT & Van Eeden FJM (2020) Bidirectional crosstalk between hypoxia-inducible factor and glucocorticoid signalling in zebrafish larvae. *PLoS Genet* 16: 1–28
- McGarry JD & Foster DW (1980) Regulation of hepatic fatty acid oxidation and ketone body production. *Annu Rev Biochem* 49: 395–420
- McKeown SR (2014) Defining normoxia, physoxia and hypoxia in tumours - Implications for treatment response. *Br J Radiol* 87: 1–12
- Minnecci PC, Deans KJ, Eichacker PQ & Natanson C (2009) The effects of steroids during sepsis depend on dose and severity of illness: An updated meta-analysis. *Clin Microbiol Infect* 15: 308–318
- Mylonis I, Simos G & Paraskeva E (2019) Hypoxia-Inducible Factors and the Regulation of Lipid Metabolism. *Cells* 8: 1–16
- Nakayama K & Kataoka N (2019) Regulation of gene expression under hypoxic conditions. *Int J Mol Sci* 20: 1–15
- Nishiyama Y, Goda N, Kanai M, Niwa D, Osanai K, Yamamoto Y, Senoo-Matsuda N, Johnson RS, Miura S, Kabe Y, *et al* (2012) HIF-1 α induction suppresses excessive lipid accumulation in alcoholic fatty liver in mice. *J Hepatol* 56: 441–447
- Park JY, Hwang TK, Park HK & Ahn RS (2014) Differences in cardiovascular and hypothalamic-pituitary-adrenal axis functions between high-altitude visitors and natives during a trek on the Annapurna circuit. *Neuroendocrinology* 99: 130–138

- Pavek P (2016) Pregnane X receptor (PXR)-mediated gene repression and cross-talk of PXR with other nuclear receptors via coactivator interactions. *Front Pharmacol* 7: 1–16
- Raff H, Jacobson L & Cullinan WE (2007) Augmented hypothalamic corticotrophin-releasing hormone mRNA and corticosterone responses to stress in adult rats exposed to perinatal hypoxia. *J Neuroendocr* 19: 907–912
- Rankin EB, Rha J, Selak MA, Unger TL, Keith B, Liu Q & Haase VH (2009) Hypoxia-Inducible Factor 2 Regulates Hepatic Lipid Metabolism. *Mol Cell Biol* 29: 4527–4538
- Ratman D, Mylka V, Bougarne N, Pawlak M, Caron S, Hennuyer N, Paumelle R, De Cauwer L, Thommis J, Rider MH, *et al* (2016) Chromatin recruitment of activated AMPK drives fasting response genes co-controlled by GR and PPAR α . *Nucleic Acids Res* 44: 10539–10553
- Reichardt HM, Kaestner KH, Tuckermann J, Kretz O, Wessely O, Bock R, Gass P, Schmid W, Herrlich P, Angel P, *et al* (1998) DNA binding of the glucocorticoid receptor is not essential for survival. *Cell* 93: 531–541
- Rock PB, Johnson TS, Larsen RF, Fulco CS, Trad LA & Cymerman A (1989) Dexamethasone as prophylaxis for acute mountain sickness. Effect of dose level. *Chest* 95: 568–573
- Rose AJ & Herzig S (2013) Metabolic control through glucocorticoid hormones: An update. *Mol Cell Endocrinol* 380: 65–78
- Rose AJ, Vegiopoulos A & Herzig S (2010) Role of glucocorticoids and the glucocorticoid receptor in metabolism: Insights from genetic manipulations. *J Steroid Biochem Mol Biol* 122: 10–20
- Schofield CJ & Ratcliffe PJ (2004) Oxygen sensing by HIF hydroxylases. *Nat Rev Mol Cell Biol* 5: 343–354
- Semenza GL (2011) Regulation of metabolism by hypoxia-inducible factor 1. *Cold Spring Harb Symp Quant Biol* 76: 347–353
- Sevilla LM & Pérez P (2018) Glucocorticoid Receptor Signaling in Skin Barrier Function. *Intech*: 13
- Spiga F, Walker JJ, Terry JR & Lightman SL (2014) HPA axis-rhythms. *Compr Physiol* 4: 1273–1298
- Steidl C, Leimeister C, Klamt B, Maier M, Nanda I, Dixon M, Clarke R, Schmid M & Gessler M (2000) Characterization of the human and mouse HEY1, HEY2, and HEYL genes: Cloning, mapping, and mutation screening of a new bHLH gene family. *Genomics* 66: 195–203
- Sterne JAC, Murthy S, Diaz J V., Slutsky AS, Villar J, Angus DC, Annane D, Azevedo LCP, Berwanger O,

- Cavalcanti AB, *et al* (2020) Association between Administration of Systemic Corticosteroids and Mortality among Critically Ill Patients with COVID-19: A Meta-analysis. *JAMA - J Am Med Assoc* 324: 1330–1341
- Taylor A (2011) High-altitude illnesses: Physiology, risk factors, prevention, and treatment. *Rambam Maimonides Med J* 2: 1–18
- Timmermans S, Souffriau J & Libert C (2019) A general introduction to glucocorticoid biology. *Front Immunol* 10: 1–17
- Uhlenhaut NH, Barish GD, Yu RT, Downes M, Karunasiri M, Liddle C, Schwalie P, Hübner N & Evans RM (2013) Insights into Negative Regulation by the Glucocorticoid Receptor from Genome-wide Profiling of Inflammatory Cistromes. *Mol Cell* 49: 158–171
- Vanderhaeghen T, Beyaert R & Libert C (2021) Bidirectional Crosstalk Between Hypoxia Inducible Factors and Glucocorticoid Signalling in Health and Disease. *Front Immunol* 12: 1–19
- Vandewalle J & Libert C (2020) Glucocorticoids in Sepsis: To Be or Not to Be. *Front Immunol* 11: 1–14
- Vandewalle J, Luypaert A, Bosscher K De & Libert C (2018) Therapeutic Mechanisms of Glucocorticoids. *Trends Endocrinol Metab* 29: 42–54
- Vandewalle J, Timmermans S, Paakinaho V, Vancraeynest L, Dewyse L, Vanderhaeghen T, Wallaey C, Van Wyngene L, Van Looveren K, Nuyttens L, *et al* (2021) Combined glucocorticoid resistance and hyperlactatemia contributes to lethal shock in sepsis. *Cell Metab* 33: 1–14
- Vegiopoulos A & Herzig S (2007) Glucocorticoids, metabolism and metabolic diseases. *Mol Cell Endocrinol* 275: 43–61
- Vettori A, Greenald D, Wilson GK, Peron M, Facchinello N, Markham E, Sinnakaruppan M, Matthews LC, McKeating JA, Argenton F, *et al* (2017) Glucocorticoids promote Von Hippel Lindau degradation and Hif-1 α stabilization. *Proc Natl Acad Sci* 114: 9948–9953
- Wagner AE, Huck G, Stiehl DP, Jelkmann W & Hellwig-Bürgel T (2008) Dexamethasone impairs hypoxia-inducible factor-1 function. *Biochem Biophys Res Commun* 372: 336–340
- Wang JC, Gray NE, Kuo T & Harris CA (2012a) Regulation of triglyceride metabolism by glucocorticoid receptor. *Cell Biosci* 2: 1–9
- Wang XL, Suzuki R, Lee K, Tran T, Gunton JE, Saha AK, Patti ME, Goldfine A, Ruderman NB, Gonzalez FJ, *et al* (2009) Ablation of ARNT/HIF1 β in Liver Alters Gluconeogenesis, Lipogenic Gene Expression, and Serum Ketones. *Cell Metab* 9: 428–439

- Wang Y, Ma Y-Y, Song X-L, Cai H-Y, Chen J-C, Song L-N, Yang R & Lu J (2012b) Upregulations of Glucocorticoid-Induced Leucine Zipper by Hypoxia and Glucocorticoid Inhibit Proinflammatory Cytokines under Hypoxic Conditions in Macrophages. *J Immunol* 188: 222–229
- Wang Y, Nakajima T, Gonzalez FJ & Tanaka N (2020) PPARs as metabolic regulators in the liver: Lessons from liver-specific PPAR-null mice. *Int J Mol Sci* 21
- Wielockx B & Meneses A (2016) PHD2: from hypoxia regulation to disease progression. *Hypoxia*: 53
- Van Wyngene L, Vandewalle J & Libert C (2018) Reprogramming of basic metabolic pathways in microbial sepsis: therapeutic targets at last? *EMBO Mol Med* 10: e8712
- Yang N, Berry A, Sauer C, Baxter M, Donaldson IJ, Forbes K, Donn R, Matthews L & Ray D (2020) Hypoxia regulates GR function through multiple mechanisms involving microRNAs 103 and 107. *Mol Cell Endocrinol* 518: 111007
- Yasuhara M, Ohama T, Matsuki N, Saito H, Shiga J, Inoue K, Kurokawa K & Teramoto T (1991) Induction of fatty liver by fasting in suncus. *J Lipid Res* 32: 887–891
- Zhang C, Qiang Q, Jiang Y, Hu L, Ding X, Lu Y & Hu G (2015) Effects of hypoxia inducible factor-1 α on apoptotic inhibition and glucocorticoid receptor downregulation by dexamethasone in AtT-20 cells. *BMC Endocr Disord* 15: 1–9
- Zheng CR, Chen GZ, Yu J, Qin J, Song P, Bian SZ, Xu B Da, Tang XG, Huang YT, Liang X, *et al* (2014) Inhaled budesonide and oral dexamethasone prevent acute mountain sickness. *Am J Med* 127: 1001-1009.e2
- Zhu X, Liu Y, Li N & He Q (2020) Inhaled budesonide for the prevention of acute mountain sickness: A meta-analysis of randomized controlled trials. *Am J Emerg Med* 38: 1627–1634

Figure Legends

Figure 1. HIFs are activated in mouse liver during hypoxia.

(A-C) The effect of hypoxia was estimated in C57BL/6J mice (n=3) by an HRE-luciferase (HRE-luc) reporter plasmid at indicated time points. All mice were injected according to body weight. **(A)** Experimental set-up. **(B)** Imaging of luciferase activity (purple signal) in the liver of control mice and mice under normoxic and hypoxic conditions at indicated time points. Red circles indicate the region of interest selected for the measurement of the luciferase activity. **(C)** Bioluminescent photon counts normalized to the PBS control group in liver of mice in normoxia and hypoxia at indicated time points. P-values were calculated using one-way ANOVA followed by post-hoc Tukey's test to correct for multiple testing during the pairwise multiple comparisons.

(D, E) Imaging of luciferase activity in the liver of HIF1a^{AlbKO} **(D)** and HIF2a^{AlbKO} **(E)** mice after a hydrodynamic tail vein injection with a HRE-luc reporter plasmid or control (PBS) according to body weight followed by 6h normoxia or hypoxia.

(F, G) Bioluminescent photon counts normalized to the PBS control group in liver of **(F)** HIF1a^{AlbKO} and **(G)** HIF2a^{AlbKO} mice and their wild-type littermates 6h after normoxia of hypoxia.

Data information: All bars represent mean \pm SEM. Each individual data point represent individual mice. P-values were calculated using two-way ANOVA followed by post-hoc Šídák's multiple comparisons test to correct for multiple testing during the pairwise multiple comparisons, except if otherwise stated. *** P<0.001; ** P \leq 0.01; * P \leq 0.05. N = normoxia, H = hypoxia. Signal around the perimeter of the Petri dishes represent aspecific luciferase signal.

Figure 2. Hypoxia modifies the GR response to DEX.

(A) Female C57BL/6J mice were put in normoxia or hypoxia for 6h or 24h, injected i.p. with PBS or DEX (10 mg/kg) and livers were isolated after 2h for genome-wide transcriptomics via RNA-seq. N=3 per group for a single RNA-seq.

(B) Venn diagram depicting the number of genes upregulated (up, LFC > 1 and P \leq 0.05) and downregulation (dn, LFC < -1 and P \leq 0.05) by DEX in normoxia and hypoxia after 6h.

(C) Scatter plot showing log fold change (LFC) of all DEX-upregulated genes (LFC > 1 and P \leq 0.05) and DEX-downregulated genes (LFC < -1 and P \leq 0.05) in normoxia vs hypoxia after 6h. The black line represents the diagonal, and the red line represents the real slope \pm standard error of the data as analysed by linear regression.

(D) Venn diagram depicting the number of genes upregulated (up, $LFC > 1$ and $P \leq 0.05$) and downregulation (dn, $LFC < -1$ and $P \leq 0.05$) by DEX in normoxia and hypoxia after 24h.

(E) Scatter plot showing log fold change (LFC) of all DEX-upregulated genes ($LFC > 1$ and $P \leq 0.05$) and DEX-downregulated genes ($LFC < -1$ and $P \leq 0.05$) in normoxia vs hypoxia after 24h. The black line represents the diagonal, and the red line represents the real slope \pm standard error of the data as analysed by linear regression.

(F, G) Examples of GR-responsive genes based on the RNA-seq data 6h **(F)** and 24h **(G)** after normoxia or hypoxia and DEX stimulation.

(H and I) ChIP-seq on liver derived from mice which were subjected to hypoxia (6h and 24h), followed by DEX (10 mg/kg) injection and 2h later sacrificed for liver isolation. **(H)** Box plots showing the LFC of genes responsive to DEX in both normoxia or hypoxia (6h and 24h). The central band represents the median. The box ranges from the first quartile (Q1) to the third quartile (Q3) which represents the interquartile range ($IQR = Q3 - Q1$) and covers the central 50% of the data. The whiskers illustrate the minimum ($Q1 - 1.5 \cdot IQR$) and maximum ($Q3 + 1.5 \cdot IQR$) of the data. Outliers are shown as dots. N=3 biological replicates per condition. **(I)** Histogram with coverage per position in a region 350 bp up- and downstream of the peaks found in normoxia and hypoxia after DEX stimulation (N_DEX, H06_DEX and H24_DEX).

Data information: All bars represent mean \pm SEM. N=3 per group. P-values were calculated using two-way ANOVA followed by post-hoc Šídák's multiple comparisons test to correct for multiple testing during the pairwise multiple comparisons, except if otherwise stated. *** $P < 0.001$, ** $P < 0.01$.

Figure 3. Induction of specific DEX responsive genes in hypoxia.

Female C57BL/6J mice were put in normoxia or hypoxia for 6h or 24h, injected i.p. with PBS or DEX (10 mg/kg) and livers were isolated for genome-wide transcriptomics via RNA-seq. N=3 per group for a single RNA-seq.

(A, B) Examples of DEX-responsive genes in hypoxia 6h **(A)** and 24h **(B)** which were not induced by DEX in normoxia.

(C-E) ChIP-seq on liver derived from mice which were subjected to hypoxia (6h and 24h), followed by DEX (10 mg/kg) injection and 2h later sacrificed for liver isolation. **(C)** Box plots showing the LFC of genes responsive to DEX in hypoxia, but not in normoxia (6h and 24h). The central band represents the median. The box ranges from Q1 to Q3 which represents the interquartile range ($IQR = Q3 - Q1$) and covers the central 50% of the data. The whiskers illustrate the minimum ($Q1 - 1.5 \cdot IQR$) and

maximum (Q3 + 1.5*IQR) of the data. Outliers are shown as dots. N=3 biological replicates per condition.

(D) Histogram showing the coverage per position in a region 350 bp up- and downstream of the GR DNA-binding peaks found in hypoxia after PBS or DEX stimulation. **(E)** Examples of specific GR DNA-binding peaks, associated with the DEX-induced gene *Slc22a5* in hypoxia (6h and 24h).

(F) HIF1aHIF2a^{fl/fl} and HIF1aHIF2a^{AlbKO} mice were put in hypoxia for 6h and stimulated with DEX. *Slc25a30* expression was measured in the liver via RT-qPCR. N=3 per group, one experiment.

Data information: All bars represent mean ± SEM. P-values were calculated using two-way ANOVA followed by post-hoc Šidák's multiple comparisons test to correct for multiple testing during the pairwise multiple comparisons, except if otherwise stated. ***P<0.001, **P<0.01, *P≤0.05.

Figure 4. Hypoxia causes activation of GR by HPA axis stimulation.

(A, B) The effect of hypoxia on the GR response to DEX stimulation was studied via RNA-seq, n=3 per group. Venn diagram depicting the number of genes upregulated (up) or downregulated (dn) by DEX in normoxia and by hypoxia after 6h **(A)** or 24h **(B)** (LFC > 1 or LFC < -1 and P ≤ 0.05).

(C) Heatmap representing log₂ values of shared stress GRE genes (counts) induced by hypoxia 6h and 24h and induced by DEX in normoxia (LFC > 1 and P ≤ 0.05).

(D-G) Female C57BL/6J and ADX mice were put in normoxia or hypoxia for 6h or 24h, n=6/group, two independent experiments. **(D, E)** Confirmation of RNA-seq data via RT-qPCR [6h **(D)** or 24h **(E)**]. **(F, G)** Plasma GC concentration [6h **(F)** or 24h **(G)**].

(H-J) Female C57BL/6J mice were put in normoxia or hypoxia for the indicated time points (2h, 6h and 24h). **(H)** Hypothalamic *Crh* mRNA expression levels were determined via RT-qPCR. **(I)** ACTH levels were measured in the plasma. N=3-5 per group, one experiment. P-values were analysed with one-way ANOVA. **(J)** Plasma GC concentration, mice in normoxia are depicted as black circles, mice in hypoxia are depicted as white squares. N=5-6 per group.

(K) Female C57BL/6J mice were put in normoxia or hypoxia for 6h and injected i.p. with 5 mg RU486 or vehicle (DMSO). Liver was isolated and stress GRE gene expression was measured via RT-qPCR. N=5 per group, one experiment.

(L) Female WT and GR^{dim/dim} mice were put in normoxia or hypoxia for 6h and liver was isolated. Stress GRE gene expression was measured via RT-qPCR. N=5-9 per group, two independent experiments.

(M) HIF1aHIF2a^{fl/fl} and HIF1aHIF2a^{AlbKO} mice were put in hypoxia for 6h. Stress GRE genes were measured in the liver via RT-qPCR. N=4 per group, one experiment.

(N) Expression levels of DEX responsive genes in normoxia and unique DEX responsive genes induced by hypoxia were measured in the liver of ADX mice after DEX stimulation during hypoxia (24h) via RT-qPCR. N=3-4 per group, one experiment.

Data information: All bars represent mean \pm SEM. P-values were calculated using two-way ANOVA followed by post-hoc Šídák's multiple comparisons test to correct for multiple testing during the pairwise multiple comparisons, except if otherwise stated. ****P<0.0001, ***P<0.001, **P<0.01, *P<0.05.

Figure 5: Involvement of hypothalamic HIF1 α and HIF2 α in activation of the HPA axis during hypoxia.

(A) Female C57BL/6J mice were put in normoxia or hypoxia for 2h, hypothalamus was isolated for analyses. N=3-4 per group for a single RNA-seq. Heatmap represents genes upregulated by hypoxia (2h) (LFC > 0.3 and P \leq 0.05).

(B) HOMER motif analysis of hypoxia-induced genes (start offset: -1 kb, end offset: 50 bp downstream of TSS). Enriched motifs with their name and p-value are displayed.

(C) Female C57BL/6J mice were put in normoxia or hypoxia for the indicated time points. Hypothalamus was isolated and stress GRE genes were measured via RT-qPCR. N=4-5 per group, one experiment.

(D) HIF1 α and HIF2 α protein levels were analysed via western blot using VINCULIN as a loading control. HIF1 α and HIF2 α protein levels were quantified using FIJI and normalized to VINCULIN levels. P-values were calculated using Mann-Whitney test. N=5 biological replicates per group. N = normoxia, H = hypoxia.

(E) HIF1 α and HIF2 α expression was detected in hypothalamus samples via IHC, scale bar 50 μ m.

Data information: All bars represent mean \pm SEM. P-values were calculated using two-way ANOVA followed by post-hoc Šídák's multiple comparisons test to correct for multiple testing during the pairwise multiple comparisons, except if otherwise stated. ****P<0.0001, **P<0.01, *P<0.05.

Figure 6. Hypoxia causes white adipose tissue lipolysis leading to FFA and liver ketone body production in a GR-dependent manner.

(A) Female C57BL/6J and ADX mice were put in normoxia and hypoxia for 6h and 24h. Plasma was isolated for metabolomics analysis. The heatmap represents log₁₀ of metabolites which are significantly increased of the plasma of C57BL/6J mice (C57BL/6J P \leq 0.05 and ADX P > 0.05, LFC > 1), significantly increased in the plasma of C57BL/6J and ADX mice (C57BL/6J P \leq 0.05 and ADX P \leq 0.05,

LFC > 1), and significantly increased in the plasma of ADX mice only (C57BL/6J $P > 0.05$ and ADX $P \leq 0.05$, LFC > 1).

(B) Metabolomics analysis identifying the presence of FFAs in the plasma of C57BL/6J and ADX mice 6h after hypoxia. **N=6 per group, two independent experiments.**

(C) PPAR α gene response in the liver of C57BL/6J mice 24h after hypoxia via RT-qPCR. N=6 per group, two independent experiments.

(D-G) FFA levels and stress GRE genes were determined in the plasma and iWAT of female C57BL/6J mice injected with 5 mg RU486 or vehicle (DMSO) **(D, F)**, and in GR^{dim/dim} mice and their wild-type littermates **(E, G)** after 6h of normoxia and hypoxia. N=4-9 per group.

(H-J) Blood ketone body levels 6h after normoxia and hypoxia in female C57BL/6J and ADX mice **(H)**, in female C57BL/6J mice injected with 5 mg RU486 or vehicle (DMSO) **(I)**, and in GR^{dim/dim} mice and their wild-type littermates **(J)**. N=5-9 per group.

(K) iWAT weight of C57BL/6J and ADX mice 6h after normoxia or hypoxia. N = 5-6 per group.

Data information: All bars represent mean \pm SEM. **P-values were calculated using two-way ANOVA followed by post-hoc Šídák's multiple comparisons test to correct for multiple testing during the pairwise multiple comparisons, except if otherwise stated.** **** $P < 0.0001$, *** $P < 0.001$, ** $P < 0.01$, * $P \leq 0.05$.

Figure 7. GR shows attenuated anti-inflammatory capacity under hypoxic conditions.

(A) Female C57BL/6J mice (n=3 per group) were put in normoxia or hypoxia for 24h, injected with PBS or DEX (10 mg/kg) and 2h later, indicated organs were isolated and gene expression was measured via RT-qPCR.

(B) LPS LD₁₀₀ dose-response in female C57BL/6J mice injected with indicated LPS doses after 24h hypoxia. During the follow-up of lethality, mice remained under hypoxic conditions. N-values are indicated in the legend.

(C, D) Organ damage parameters **(C)** and GC levels **(D)** were determined in the plasma of female C57BL/6J mice injected with 14.5 mg/kg LPS (normoxia) or 5 mg/kg LPS (hypoxia) 6h and 2h after LPS injection, respectively. **N=4-5 per group.**

(E) Female C57BL/6J mice were injected with 14.5 mg/kg LPS (normoxia) or 5 mg/kg LPS (hypoxia) after 24h normoxia or hypoxia. Liver was isolated 6h after injected and typical GRE genes were measured via RT-qPCR. **N=4-5 per group.**

(F) Female ADX mice were put in normoxia or hypoxia for 24h, injected i.p. with PBS or DEX (10 mg/kg) and 2h later, liver was isolated for RT-qPCR analyses of typical GRE genes. **N=3-4 per group.**

(G) Female C57BL/6J mice were injected with 14.5 mg/kg LPS (normoxia) or 5 mg/kg LPS (hypoxia) after 24h normoxia or hypoxia, with or without pre-treatment with 10 mg/kg DEX 1h before LPS injection. During the follow-up of lethality, mice remained under normoxic or hypoxic conditions. Mice in normoxia: black circles (LPS), black squares (DEX-LPS); mice in hypoxia: white circles (LPS), white squares (DEX-LPS).

(H) Female ADX mice were injected with 0.05 mg/kg LPS after 24h normoxia or hypoxia, with or without 10 mg/kg DEX pre-treatment 1h before LPS injection. During the follow-up of lethality, mice remained under normoxic or hypoxic conditions. ADX mice in normoxia: black circles (LPS), black squares (DEX-LPS); ADX mice in hypoxia: white circles (LPS), white squares (DEX-LPS).

Data information: All bars represent mean \pm SEM. **P-values were calculated using two-way ANOVA followed by post-hoc Šídák's multiple comparisons test to correct for multiple testing during the pairwise multiple comparisons, except if otherwise stated.** Survival curves were analysed with Fisher's exact test. ****P<0.0001, ***P<0.001, **P<0.01, *P≤0.05.

Expanded View Figure Legends

Figure EV1. Hypoxia modifies the GR response to DEX in the liver.

(A) Female C57BL/6J mice were put in normoxia or hypoxia for 6h and 24h, liver was isolated for further analysis. GR protein levels were analysed via western blot using ACTIN as a loading control. GR protein levels were quantified using FIJI and normalized to ACTIN levels. P-values were calculated using one-way ANOVA. **N=4 biological replicates per group.**

(B) PCA plot visualizing the variance within samples per conditions based on the peaks found in the ChIP-seq experiment after normalization and scaling of the data.

(C) Heatmap based on the GR DNA-binding peaks after normalization and scaling of the ChIP-seq data found in normoxia after DEX stimulation compared to input samples of this group. Log₁₀ of the total area under the peak is shown.

(D, E) Examples of specific GR peaks, associated with the DEX-induced gene *Fam107a* **(D)** and *Sgk1* **(E)** in normoxia and hypoxia (6h and 24h).

(F) HIF1aHIF2a^{fl/fl} and HIF1aHIF2a^{Alb^{KO}} mice were put in hypoxia for 6h and stimulated with DEX. *Hspa1a* expression was measured in the liver via RT-qPCR. N=4 per group, one experiment.

Data information: All bars represent mean \pm SEM. P-values were calculated using two-way ANOVA followed by post-hoc Šídák's multiple comparisons test to correct for multiple testing during the pairwise multiple comparisons, except if otherwise stated. ***P<0.001, **P<0.01, *P \leq 0.05.

Figure EV2. Hypoxia itself causes the induction of GR responsive genes.

(A,B) Female C57BL/6J mice were put in normoxia or hypoxia for 6h **(A)** or 24h **(B)**, injected with PBS or DEX (10 mg/kg) and 2h later, liver was isolated for analyses. N=3 per group for a single RNA-seq. **(A)** Heatmap representing stress GRE genes induced by hypoxia (6h) and DEX in normoxia. Log₂ values are shown of the counts of the stress GRE genes based on the RNA-seq data (LFC > 1 and P \leq 0.05). **(B)** Heatmap representing stress GRE genes induced by hypoxia (24h) and DEX in normoxia. Log₂ values are shown of the counts of the stress GRE genes based on the RNA-seq data (LFC > 1 and P \leq 0.05).

(C,D) Females C57BL/6J and ADX mice were put in normoxia (N) and hypoxia (H, 6h and 24h) and the expression of HIF target genes were evaluated in the liver via RT-qPCR. **(C)** Fold inductions (H/N) of HIF target genes in C57BL/6J and ADX mice. **(D)** Examples of the expression levels of HIF target genes. N=3 per group.

Data information: All bars represent mean \pm SEM. P-values were calculated using two-way ANOVA followed by post-hoc Šídák's multiple comparisons test to correct for multiple testing during the pairwise multiple comparisons, except if otherwise stated. ***P<0.001, **P<0.01, *P \leq 0.05.

Figure EV3. Hypoxia causes activation of GR by HPA axis stimulation.

(A, B) Histogram showing the coverage per position in a region 350 bp up- and downstream of the peaks found in normoxia after PBS or DEX stimulation and in hypoxia 6h **(A)** and 24h **(B)**.

(C-F) Examples of specific GR peaks, associated with the DEX-induced and hypoxia induced genes *Cdkn1a* **(C)**, *Mfsd2a* **(D)**, *Ddit4* **(E)** and *Igfbp1* **(F)** in normoxia with and without DEX stimulation and in hypoxia (6h and 24h).

(G-I) Female C57BL/6J and ADX mice were put in normoxia and hypoxia (2h) and hypothalamus and blood was collected. **(G)** Hypothalamic *Crh* mRNA levels measured via RT-qPCR. **(H)** Stress GRE gene expression. **(I)** Plasma GC levels. N=3 per group.

Data information: All bars represent mean \pm SEM. P-values were calculated using two-way ANOVA followed by post-hoc Šídák's multiple comparisons test to correct for multiple testing during the

pairwise multiple comparisons, except if otherwise stated. **** $P < 0.0001$, *** $P < 0.001$, ** $P < 0.01$, * $P \leq 0.05$.

Figure EV4. Hypoxia causes white adipose tissue lipolysis leading to FFA and liver ketone body production in a GR-dependent manner.

(A) Female C57BL/6J and ADX mice were put in normoxia and hypoxia for 6h. Plasma was isolated for metabolomics analysis. The heatmap represents \log_{10} of metabolites which are significantly increased of the plasma of C57BL/6J mice (C57BL/6J $P \leq 0.05$ and ADX $P > 0.05$), significantly increased in the plasma of C57BL/6J and ADX mice (C57BL/6J $P \leq 0.05$ and ADX $P \leq 0.05$), and significantly increased in the plasma of ADX mice only (C57BL/6J $P > 0.05$ and ADX $P \leq 0.05$).

(B) Female C57BL/6J mice were put in normoxia and hypoxia for 6h and liver was isolated for analyses. PPAR α gene response in the liver of C57BL/6J mice 6h after hypoxia via RT-qPCR. N=6 per group pooled from two independent experiments.

(C) PPAR α gene response in the liver of PPAR $\alpha^{\text{Alb}^{\text{KO}}}$ mice and their wild-type littermates 24h after hypoxia via RT-qPCR. N=5 per group, one experiment.

(D) Fold inductions (DEX/PBS) of *Ppara* and PPAR α responsive genes in normoxia and hypoxia (6h and 24h) based on the RNA-seq mRNA counts. N=3 biological replicates for RNA-seq data. Fold inductions of 22 genes are depicted.

(E) FFA levels in the plasma of PPAR $\alpha^{\text{fl/fl}}$ and PPAR $\alpha^{\text{Alb}^{\text{KO}}}$ mice after 6h hypoxia. N=4-5 per group, one experiment.

(F) Metabolomics analysis identifying the presence of acetoacetic acid in the plasma of C57BL/6J and ADX mice 6h after hypoxia. N=6 per group, pooled from two independent experiments.

(G) The average food intake of C57BL/6J and ADX mice was measured after 24h normoxia or hypoxia. Pooled data of 3 independent experiments.

(H) Blood ketone body levels 6h after normoxia and hypoxia in PPAR $\alpha^{\text{fl/fl}}$ and PPAR $\alpha^{\text{Alb}^{\text{KO}}}$ mice. N = 5 per group, one experiment.

Data information: All bars represent mean \pm SEM. P-values were calculated using two-way ANOVA followed by post-hoc Šídák's multiple comparisons test to correct for multiple testing during the pairwise multiple comparisons, except if otherwise stated. **** $P < 0.0001$, *** $P < 0.001$, ** $P < 0.01$, * $P \leq 0.05$.

Figure EV5. GR shows attenuated anti-inflammatory capacity under hypoxic conditions.

Female C57BL/6J mice were put in normoxia or hypoxia for 6h, injected i.p. with PBS or DEX (10 mg/kg) and 2h later, liver was isolated for analyses. N=3 per group for a single RNA-seq.

(A,B) Heatmap representing the DEX effect on the expression of pro- and anti-inflammatory genes in normoxia and hypoxia after 6h **(A)** and 24h **(B)**. Log₂ values are shown of the counts of these genes on the RNA-seq data. Genes with known pro-inflammatory function are categorized below the black line, genes with known anti-inflammatory function are shown above the black line.

(C) LPS LD₁₀₀ dose-response was determined in female ADX mice injected with indicated LPS doses after 24h hypoxia. During the follow-up of lethality, mice remained under hypoxic conditions. N-values are indicated in the legend.

(D-G) Female C57BL/6J mice were put in normoxia **(D, F)** or hypoxia **(E, G)** for 24h, injected with PBS or DEX (10 mg/kg) and 1h later injected with 14.5 mg/kg LPS (normoxia) or 5 mg/kg (hypoxia). Organ damage parameters **(D, E)** were determined in the plasma of the mice 24h after LPS injection. **N=11-12 per group.** Glucose levels **(F, G)** were measured via the tail vein. **N=6 per group.**

Data information: All bars represent mean ± SEM. P-value were analysed with one-way ANOVA. **Survival curves were analysed with Fisher's exact test.** ****P<0.0001, ***P<0.001, **P<0.01, *P≤0.05.

Table 1. Enrichr pathway analysis based on genes induced by DEX in normoxia alone and genes induced by DEX in both normoxia and hypoxia.

N_DEX only		N_DEX_H_DEX	
Name	P-value	Name	P-value
Regulation of Cardiac Hypertrophy by miR-208 WP1526	0.00729	p53 signaling WP2902	0.00048
MAPK signaling pathway WP493	0.01072	Adipogenesis genes WP447	0.00089
Signal Transduction of S1P Receptor WP57	0.01306	White fat cell differentiation WP2872	0.01170
Irinotecan Pathway WP475	0.02059	Calcium Regulation in the Cardiac Cell WP553	0.022662
Macrophage markers WP2271	0.02059	Myometrial Relaxation and Contraction Pathways WP385	0.02691
Gene regulatory network modelling somitogenesis WP2852	0.02480	ErbB signaling pathway WP1261	0.03079
Exercise-induced Circadian Regulation WP544	0.02504	Notch Signaling Pathway WP29	0.03079
IL-6 signaling Pathway WP387	0.02555	Insulin Signaling WP65	0.03165
Neural Crest Differentiation WP2074	0.02784	MAPK signaling pathway WP493	0.03165
Adipogenesis genes WP447	0.03372	Apoptosis WP1254	0.03253

Wiki Pathways 2019 Mouse analysis of the 6h + 24h genes that are induced by DEX in normoxia only (N_DEX) or in normoxia and hypoxia (N_DEX_H_DEX). Remark that GR pathways controlling inflammation (in yellow) are lost when GR is induced in hypoxic conditions and are replaced by metabolic pathways (in green).

Table 2. Primer sequences used for RT-qPCR.

Gene	Forward primer (5'-3')	Reverse primer (5'-3')
<i>Hprt</i>	AGTGTTGGATACAGGCCAGAC	CGTGATTCAAATCCCTGAAGT
<i>Rpl</i>	CCTGCTGCTCTCAAGGTT	TGGTTGTCAGTGCCTCGTACTT
<i>Tbp</i>	GAAGCTGCGGTACAATTCCAG	CCCCTTGTACCCTTCACCAAT
<i>Fam107a</i>	CAGACCAGAGTACAGAGAGTGG	GTGGTTCATAAGCAGCTCACG
<i>Ddit4</i>	CAAGGCAAGAGCTGCCATAG	CCGGTACTTAGCGTCAGGG
<i>Cdkn1a</i>	CCTGGTGATGTCCGACCTG	CCATGAGCGCATCGCAATC
<i>Mfsd2a</i>	AGAAGCAGCAACTGTCCATTT	CTCGGCCACAAAAAGGATAAT
<i>Crh</i>	CCTCAGCCGGTTCTGATCC	AGCAACACGCGGAAAAAGTTA
<i>Ppara</i>	AGAGCCCCATCTGTCCTCTC	ACTGGTAGTCTGCAAAACCAAA
<i>Hmgcs2</i>	GAAGAGAGCGATGCAGGAAAC	GTCCACATATTGGGCTGGAAA
<i>Nfkbia</i>	TGAAGGACGAGGAGTACGAGC	TTCGTGGATGATTGCCAAGTG
<i>Dusp1</i>	GTTGTTGGATTGTCGCTCCTT	TTGGGCACGATATGCTCCAG
<i>Tsc22d3</i>	CCAGTGTGCTCCAGAAAGTGAAG	AGAAGGCTCATTGGCTCAATCTC
<i>Vdr</i>	ACCCTGGTGACTTTGACCG	GGCAATCTCCATTGAAGGGG
<i>Serpina3c</i>	CTGGGGCTCGTGATAACTGG	TCGAGTTGTGTCCCATTTTCTTT
<i>Hspa1a</i>	TGGTGAGTCCGACATGAAG	GCTGAGAGTCGTTGAAGTAGGC
<i>Slc22a5</i>	ACTGTGCCAGGGGTGCTAT	GCAACTGAGGCTTCGTAGAAT

Figure 1: HIFs are activated in mouse liver during hypoxia

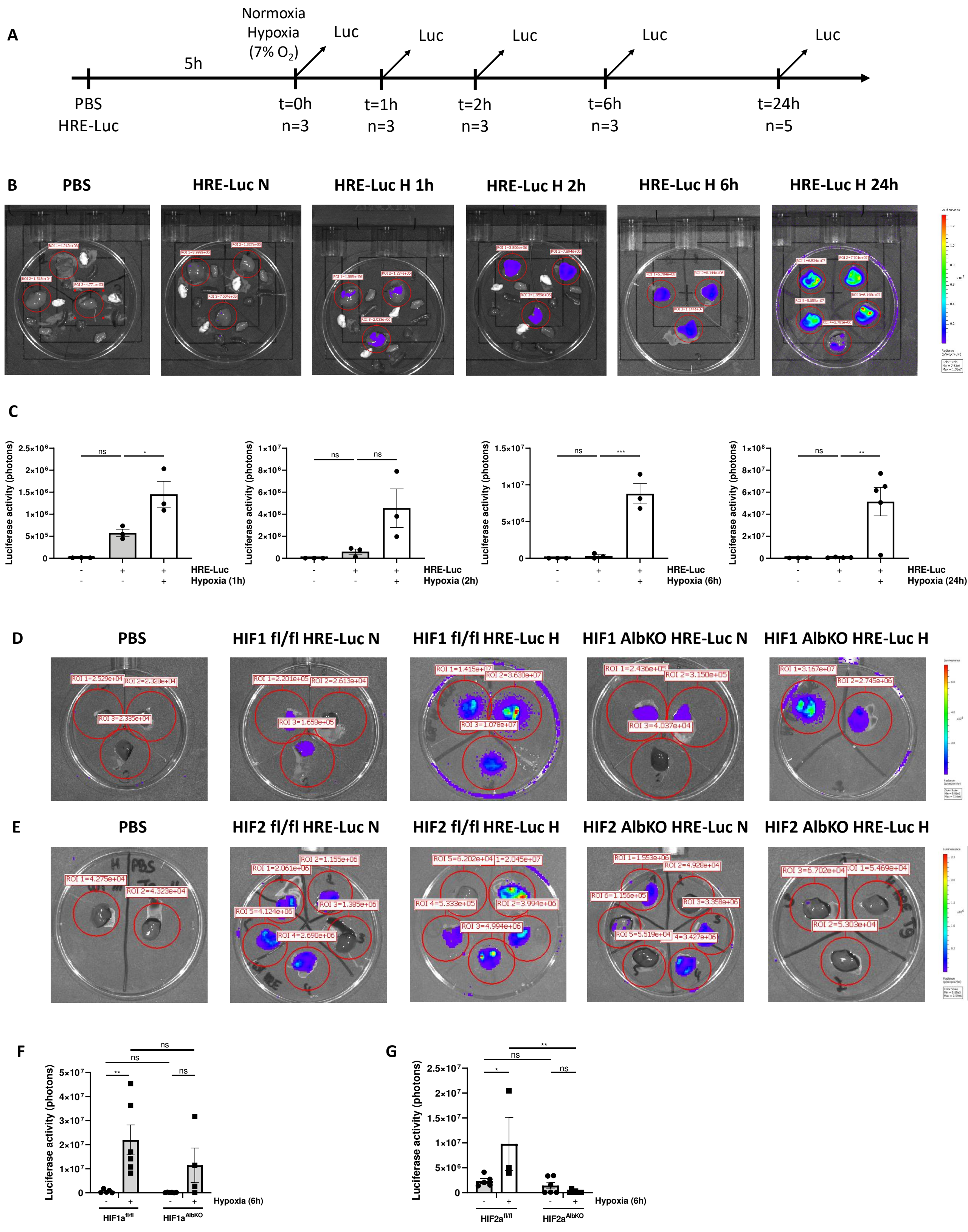
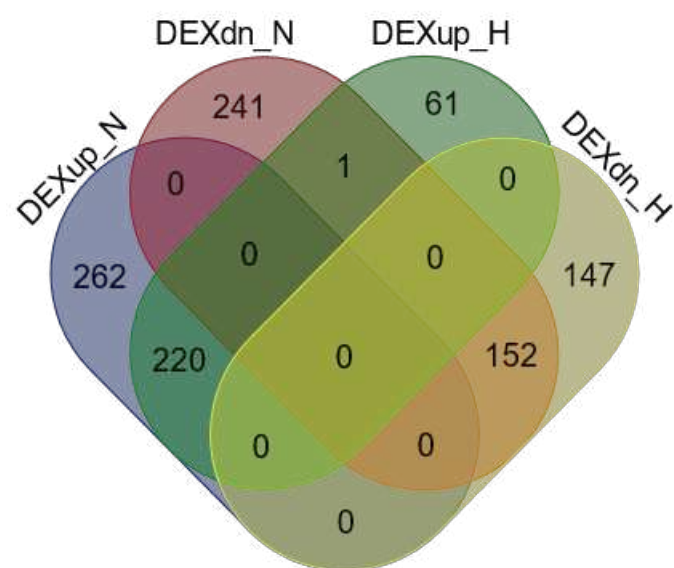


Figure 2: Hypoxia modifies the GR response to DEX in the liver

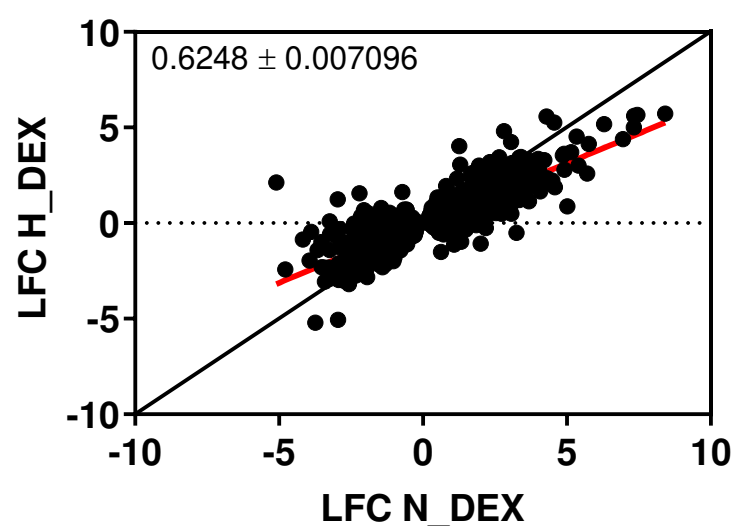
A



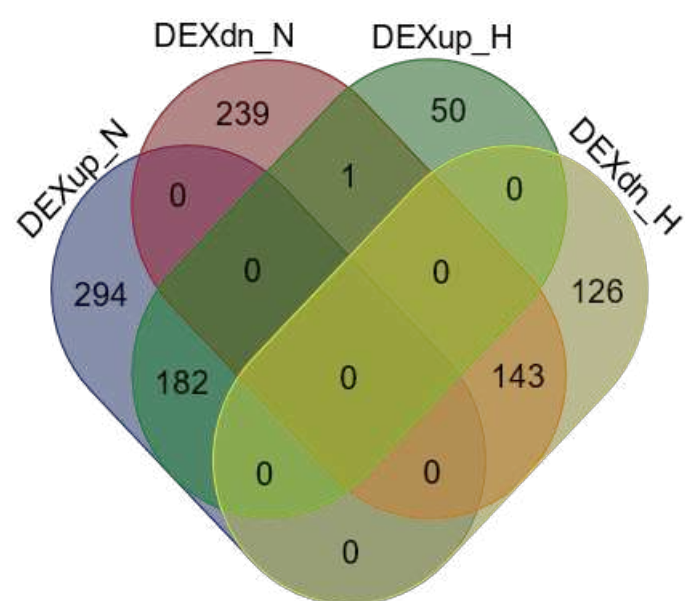
B 6h



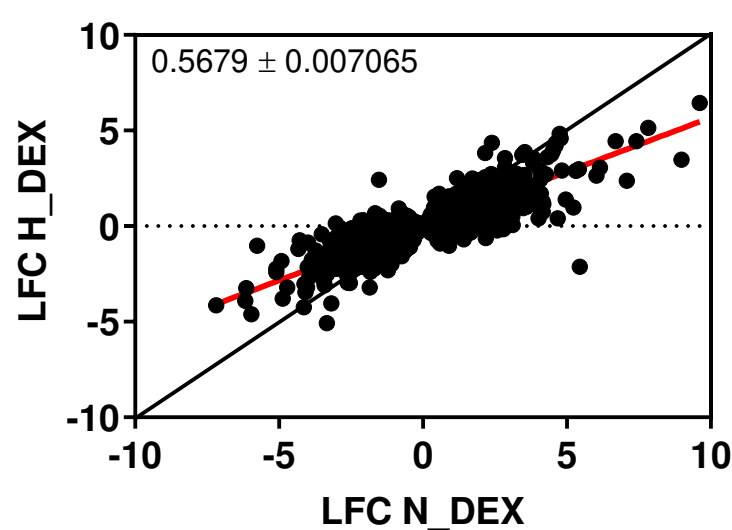
C



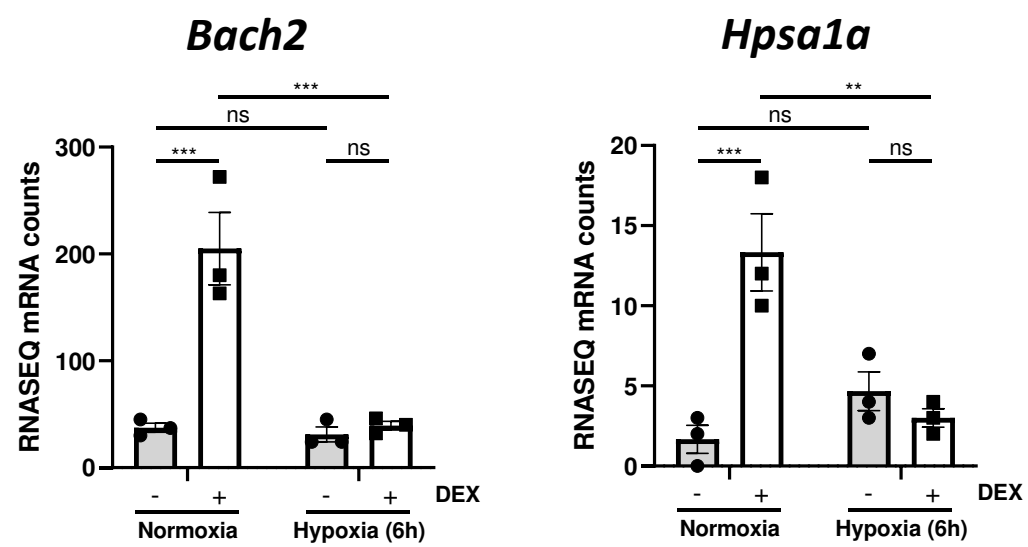
D 24h



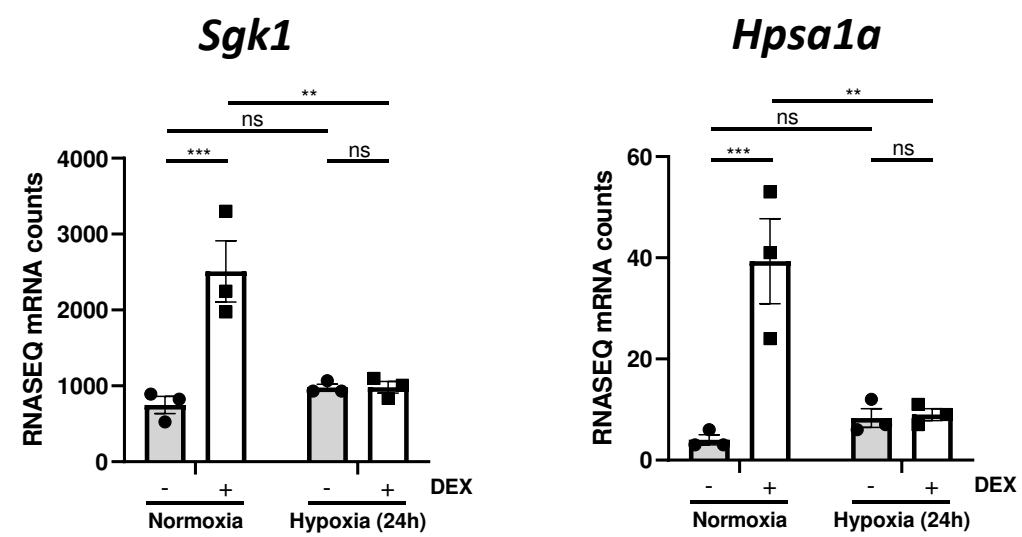
E



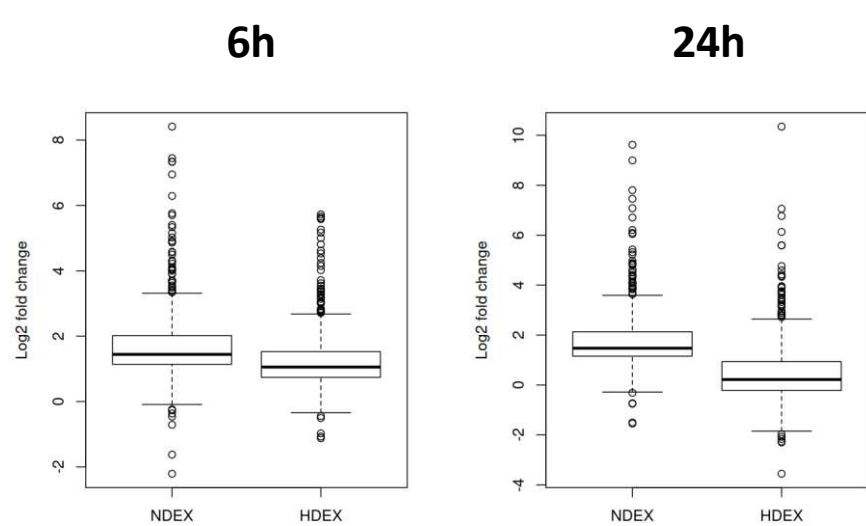
F



G



H



I

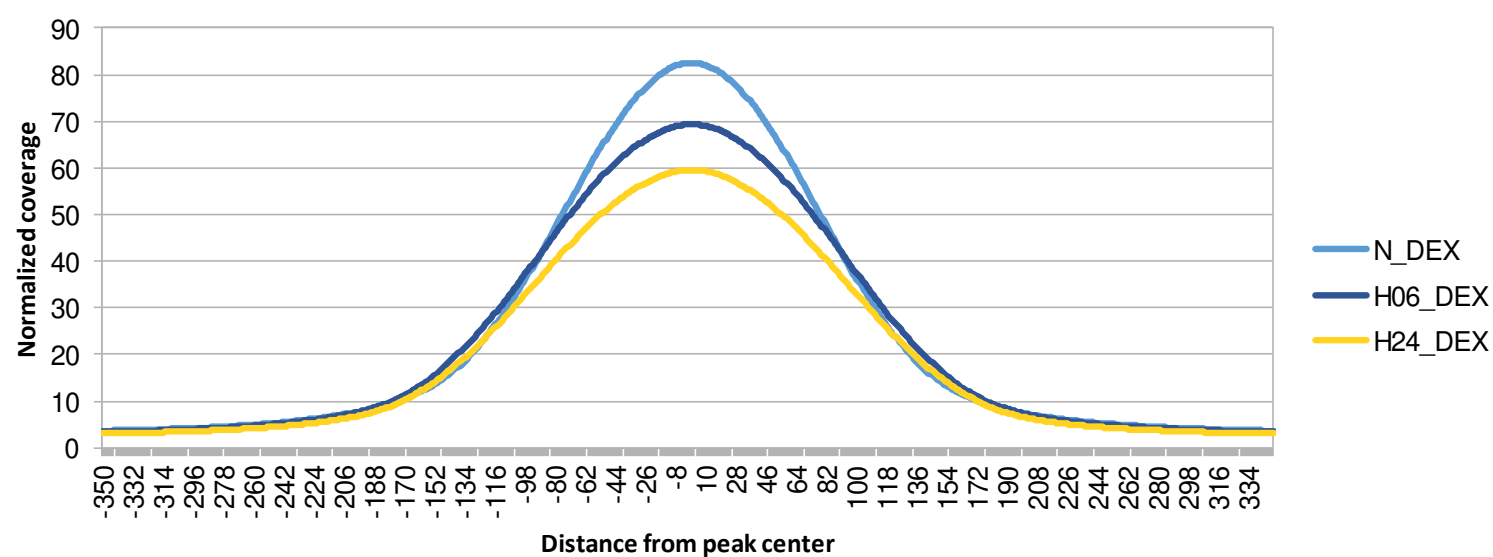


Figure 3: Induction of specific DEX responsive genes in hypoxia

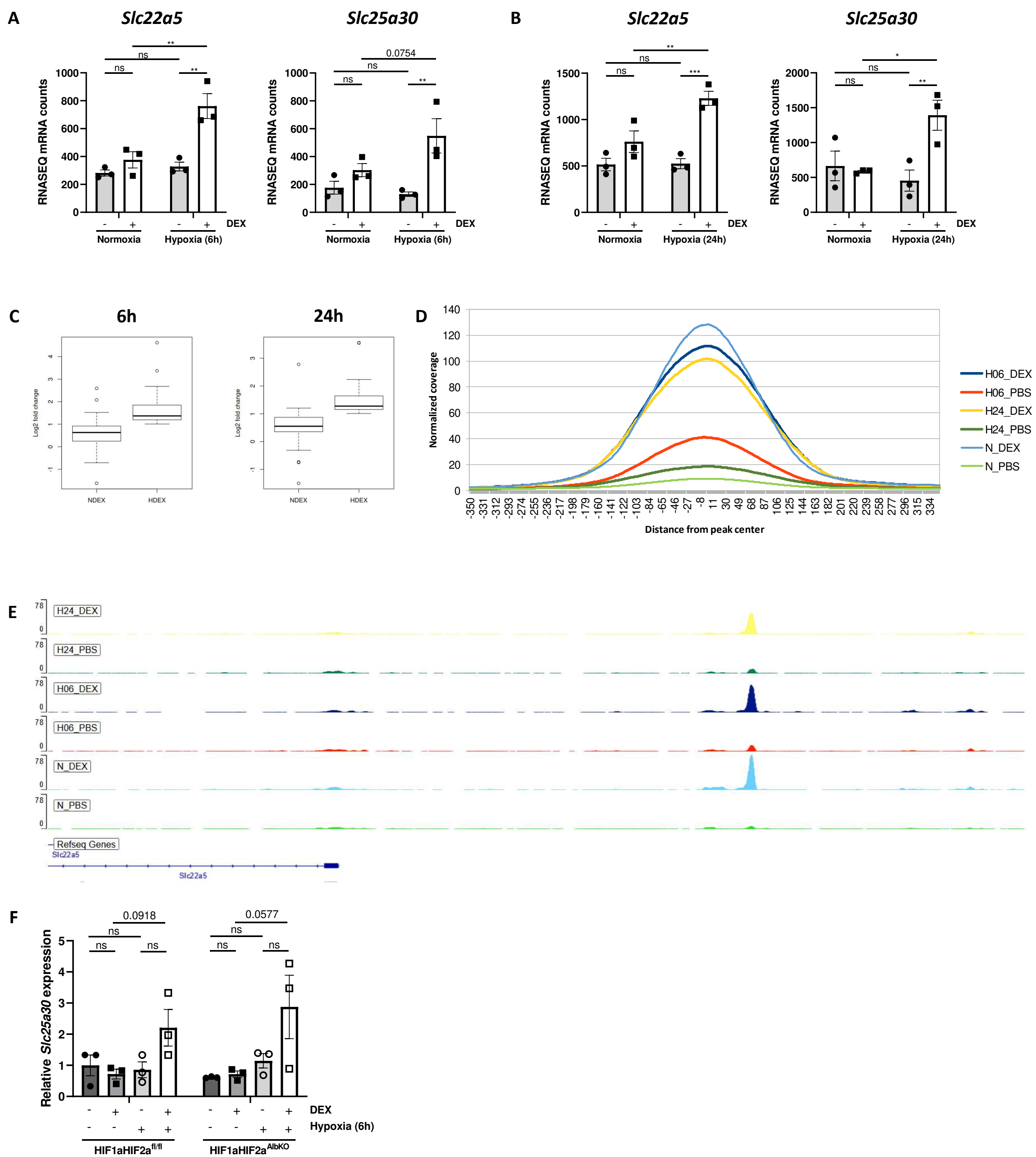


Figure 4: Hypoxia causes activation of GR by HPA axis stimulation

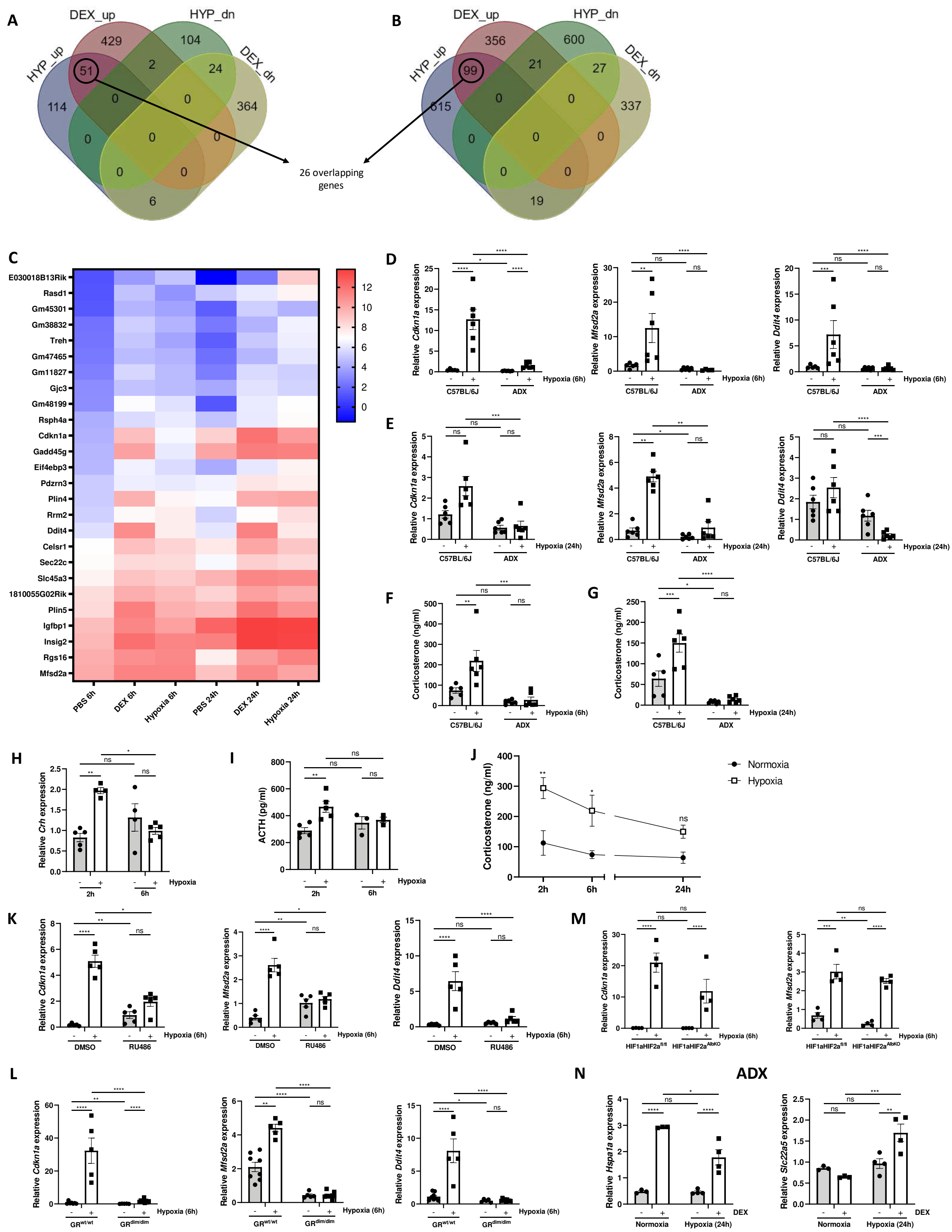
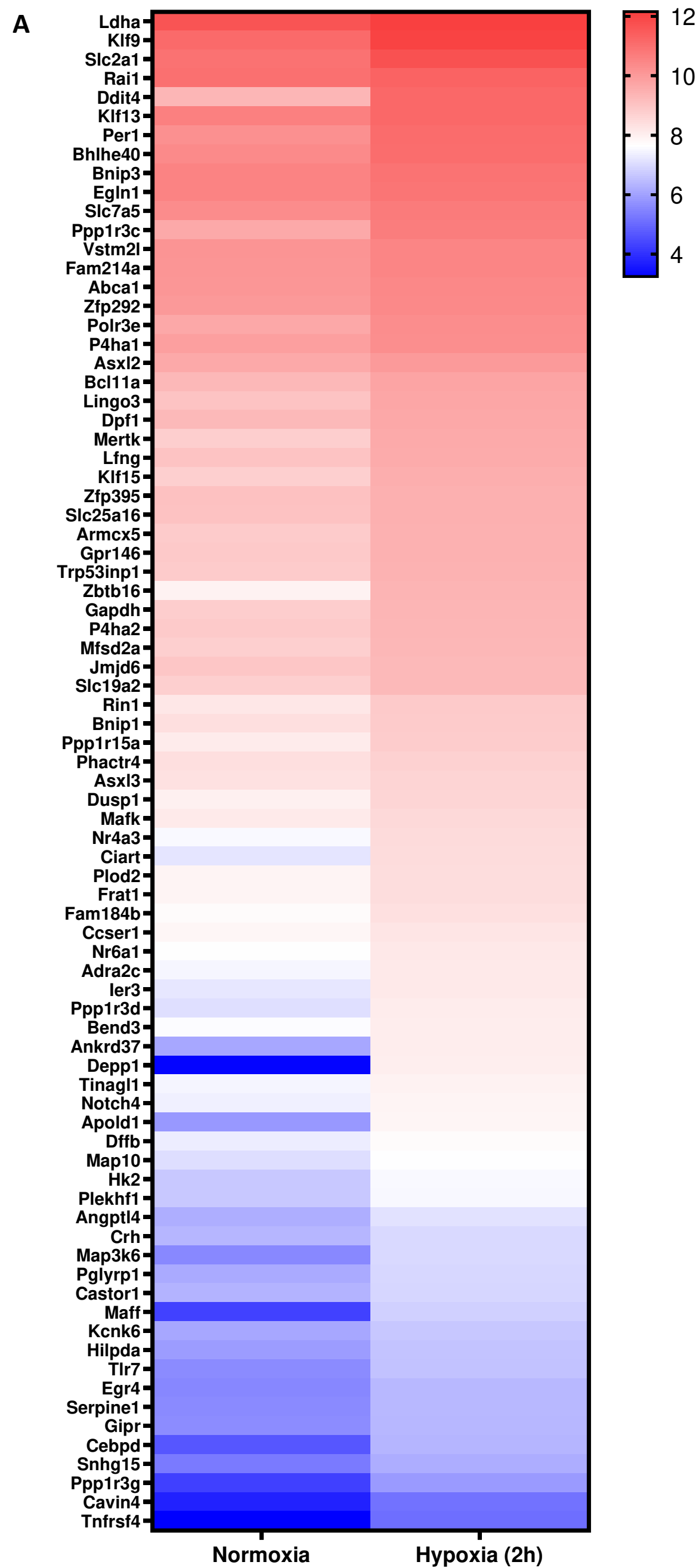


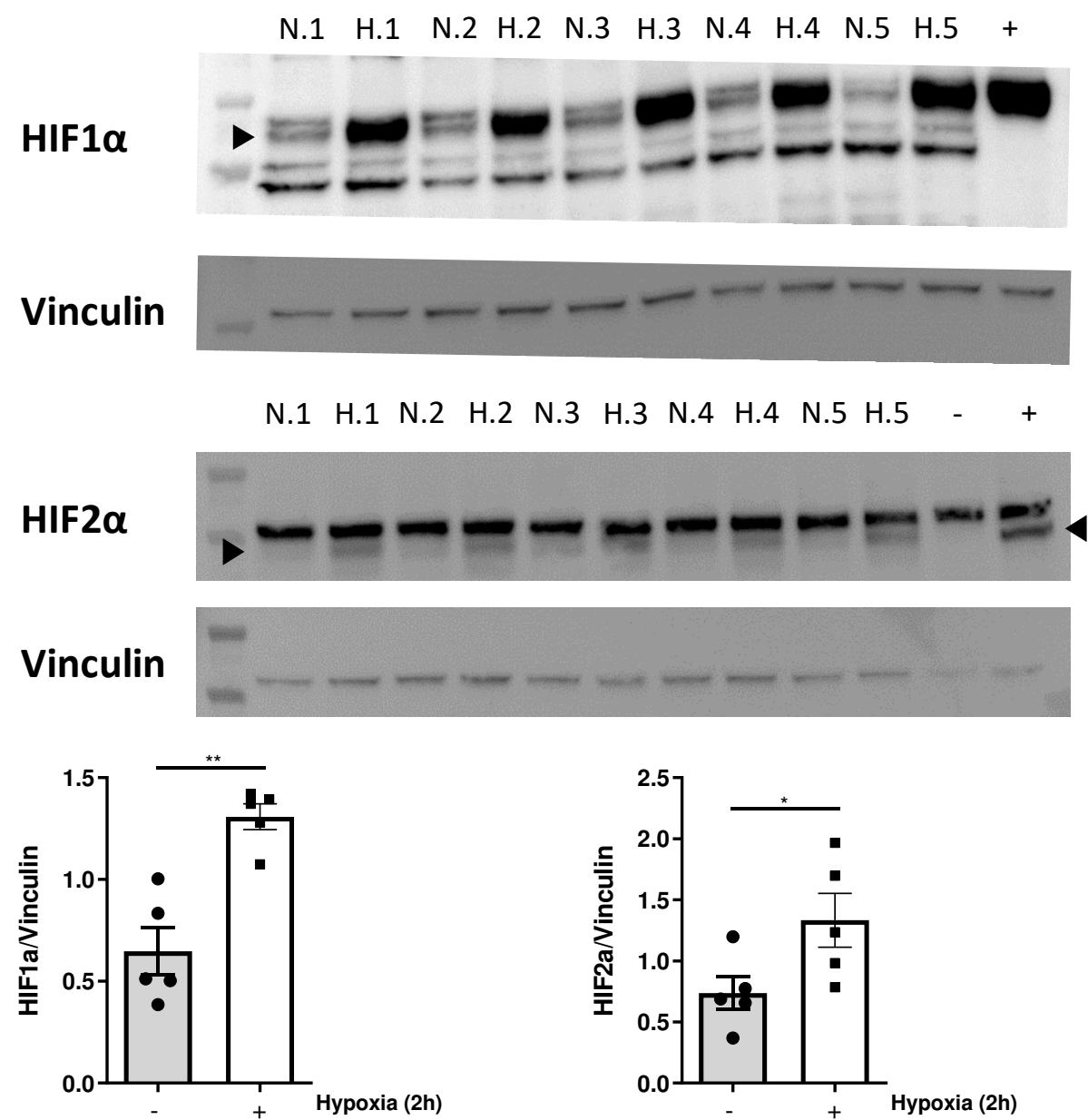
Figure 5: Involvement of hypothalamic HIF1 α and HIF2 α in activation of the HPA axis during hypoxia



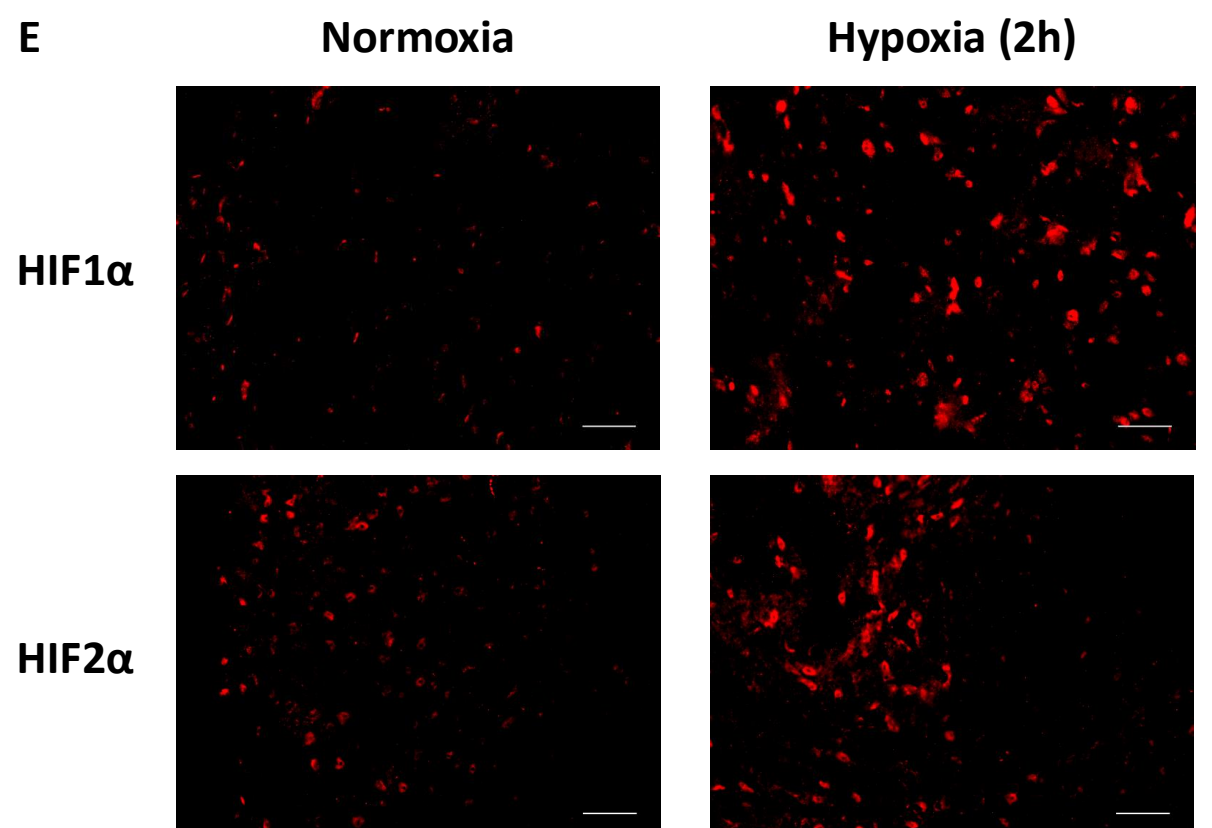
B

MOTIF	Name	P-value
	TATA-Box	1e-8
	HIF2 α	1e-4
	NPAS2	1e-4
	NPAS	1e-3
	CLOCK	1e-3
	HIF1 β	1e-3
	c-Myc	1e-2
	NF κ B-p65-Rel	1e-2
	GRE	1e-2
	MNT	1e-2
	BMAL1	1e-2
	Fos	1e-2
	ARE	1e-2
	HIF1 α	1e-2

D



E



C

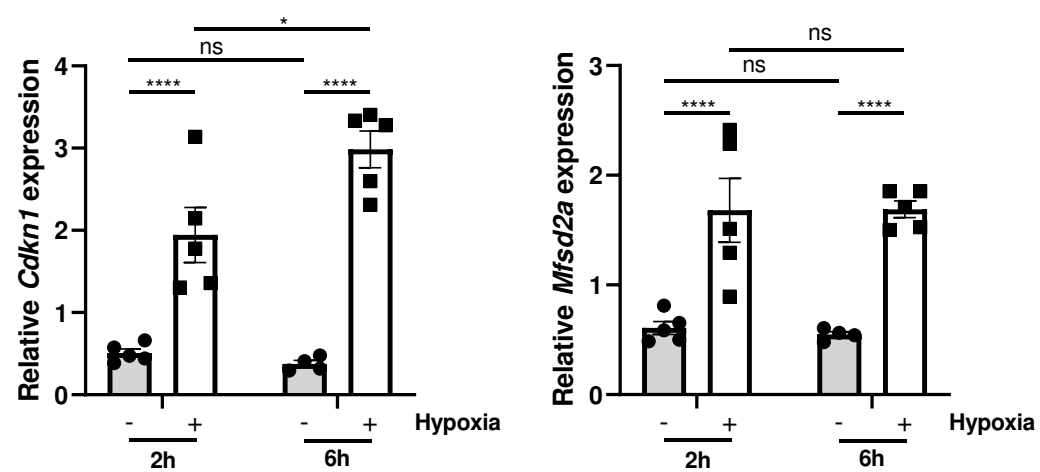


Figure 6: Hypoxia causes white adipose tissue lipolysis leading to FFA and liver ketone body production in a GR-dependent manner

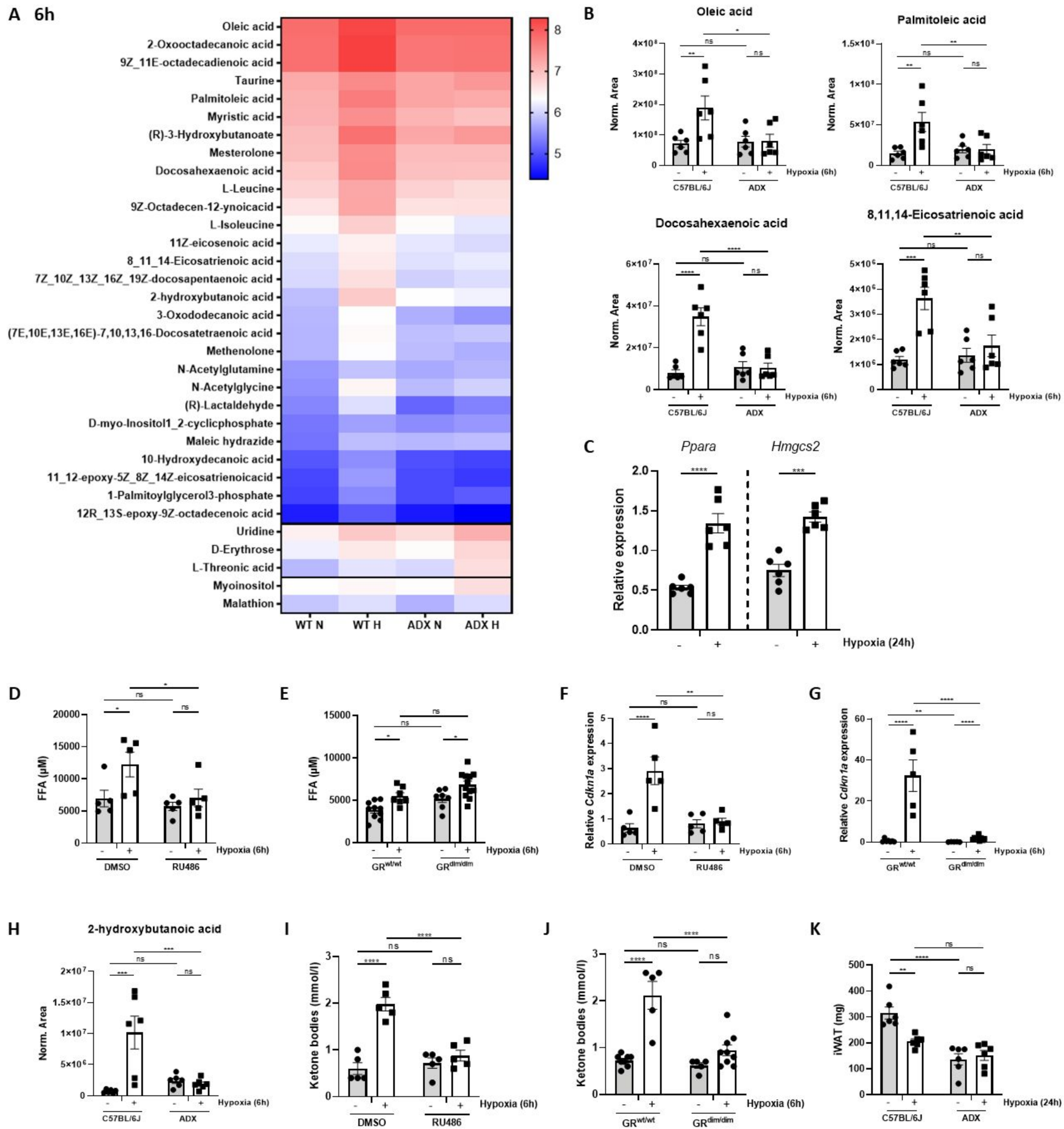


Figure 7: GR shows attenuated anti-inflammatory capacity under hypoxic conditions

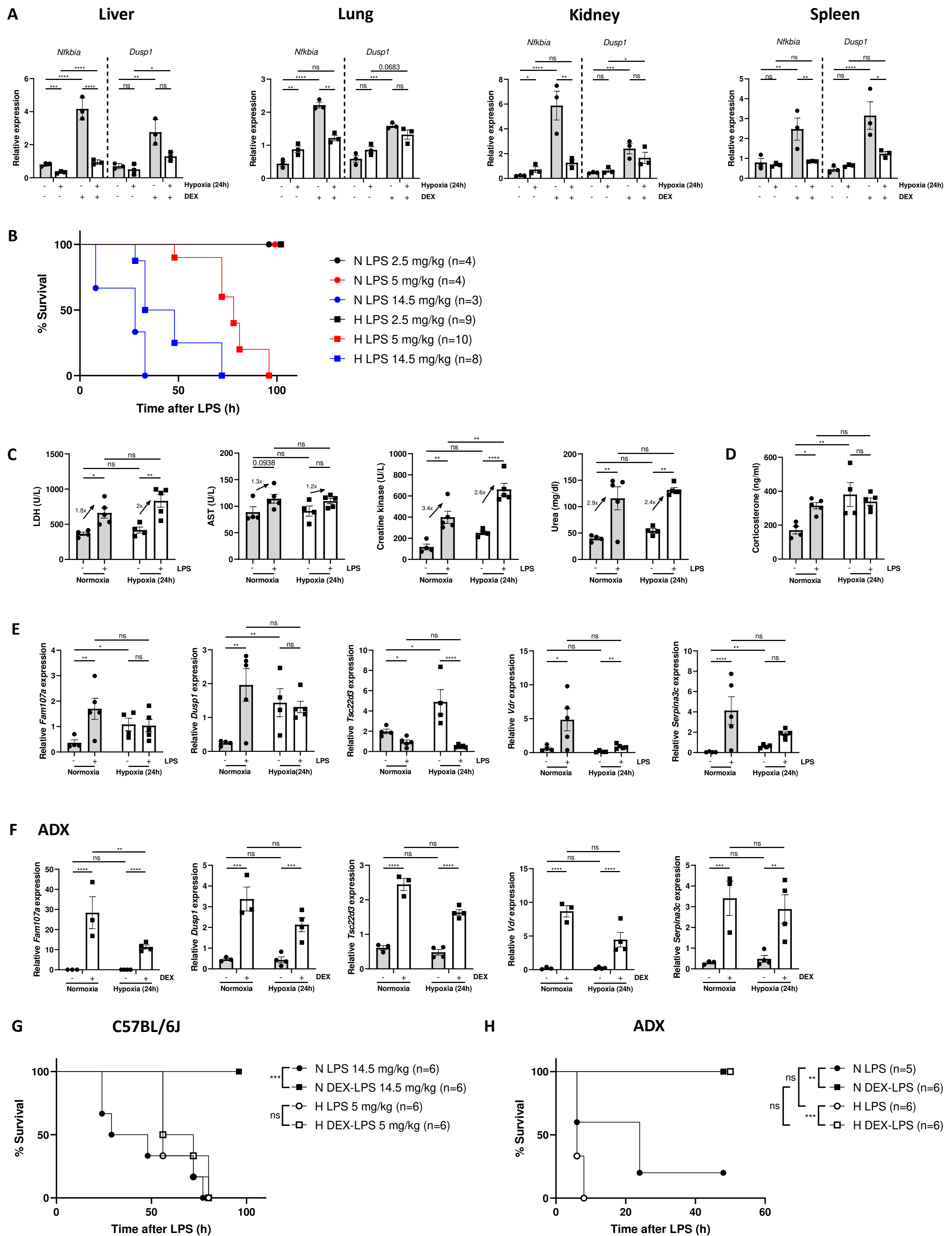


Figure EV1: Hypoxia modifies the GR response to DEX in the liver.

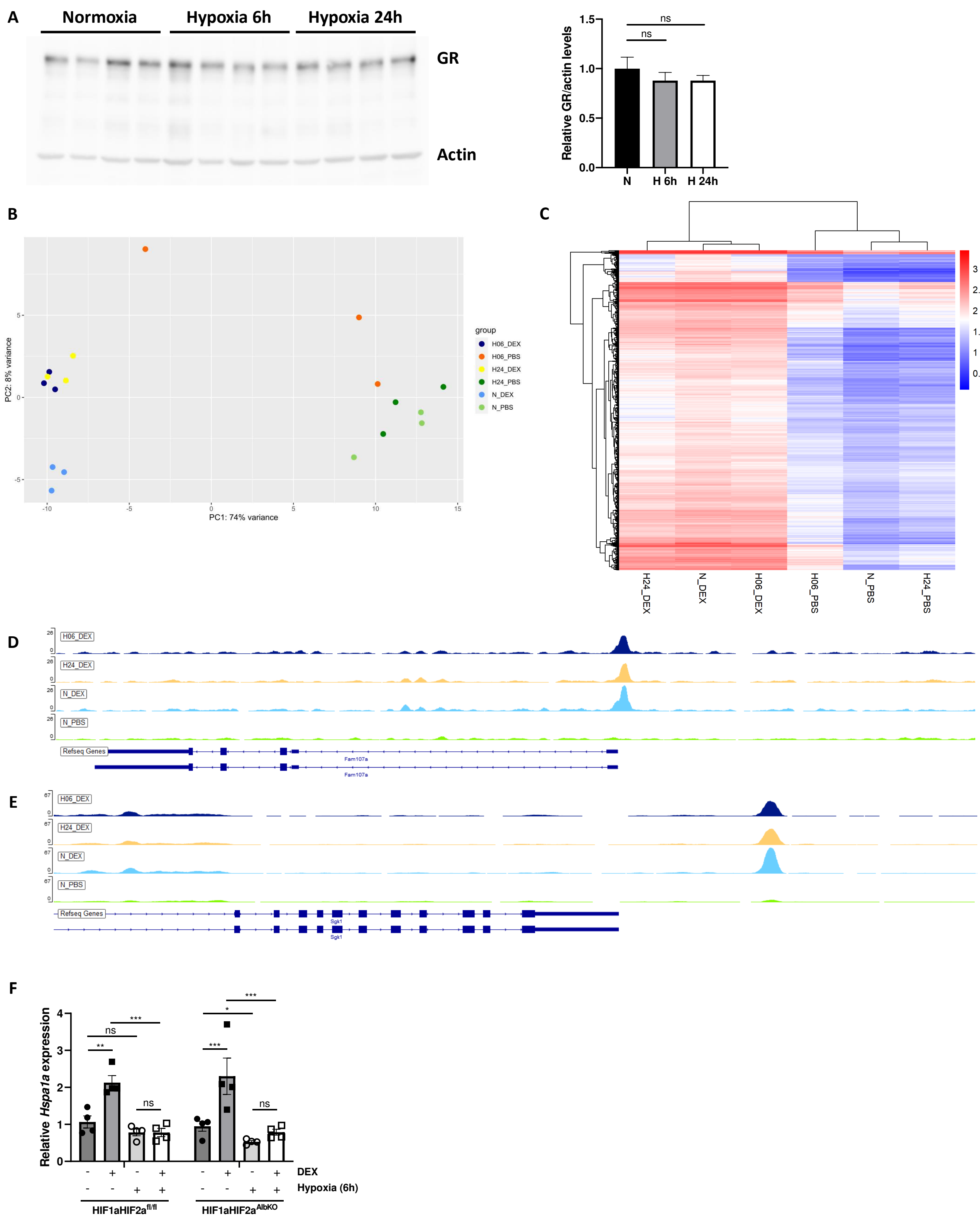


Figure EV2: Hypoxia itself causes the induction of GR responsive genes

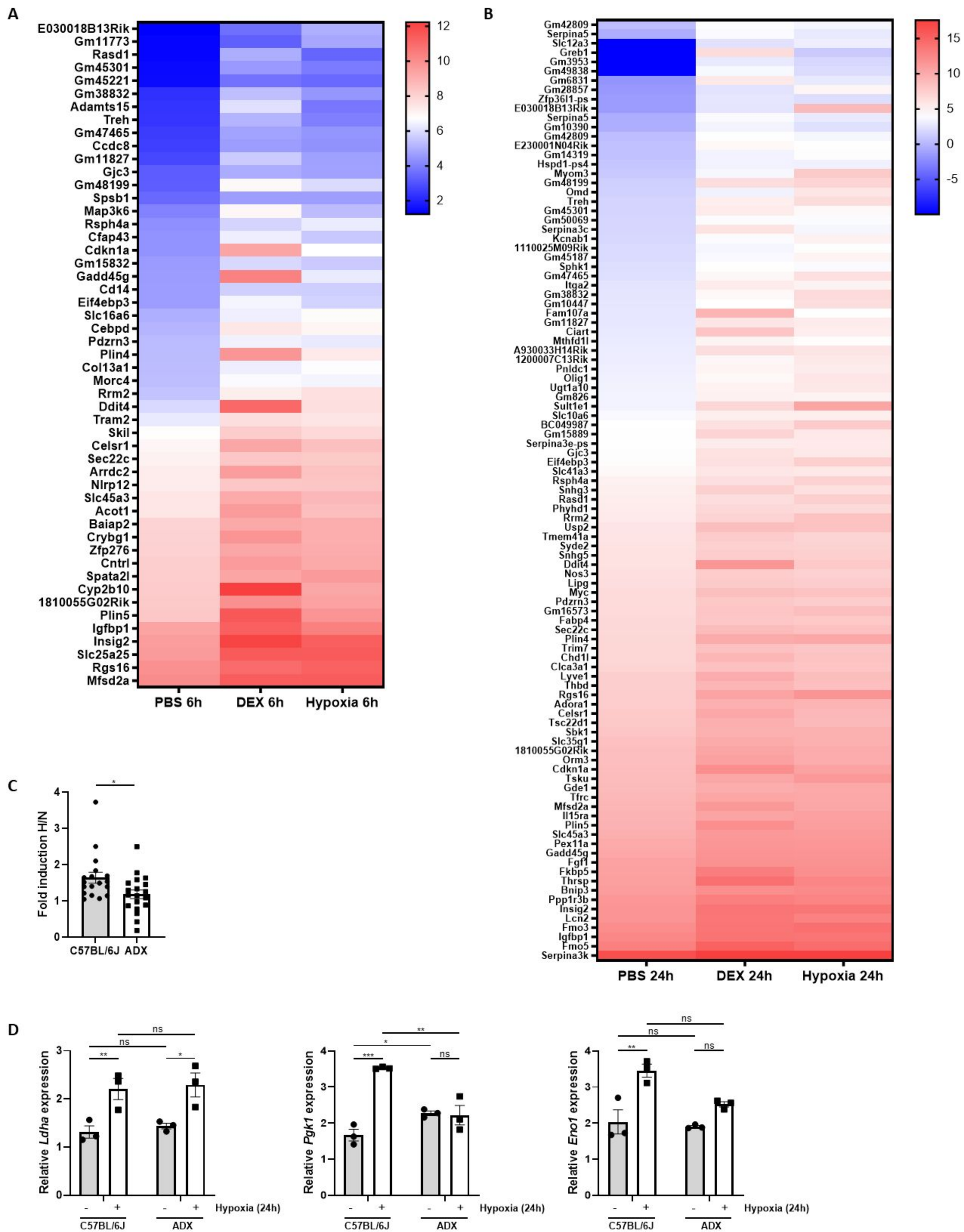


Figure EV3: Hypoxia causes activation of GR by HPA axis stimulation

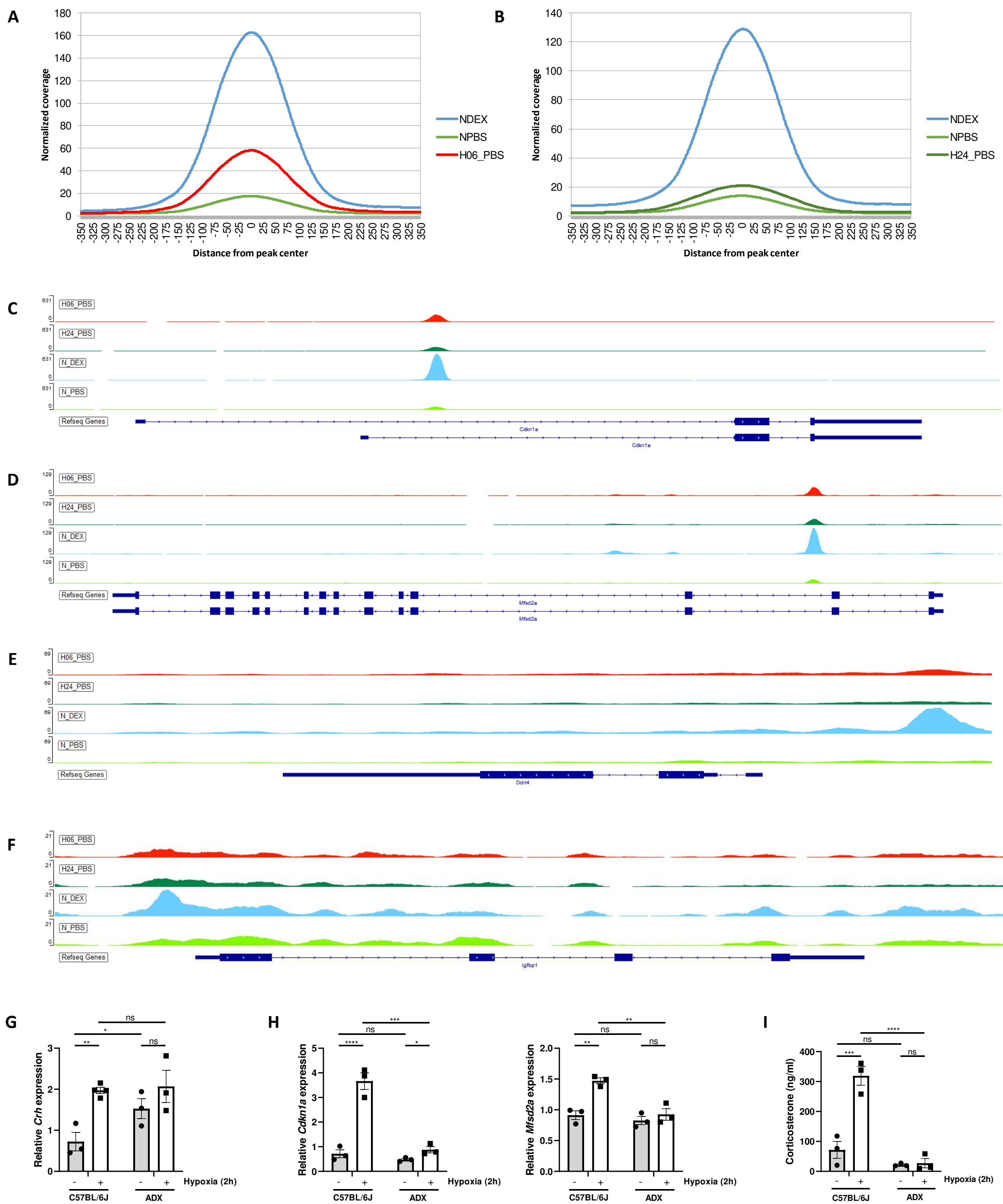


Figure EV4: Hypoxia causes white adipose tissue lipolysis leading to FFA and liver ketone body production in a GR-dependent manner

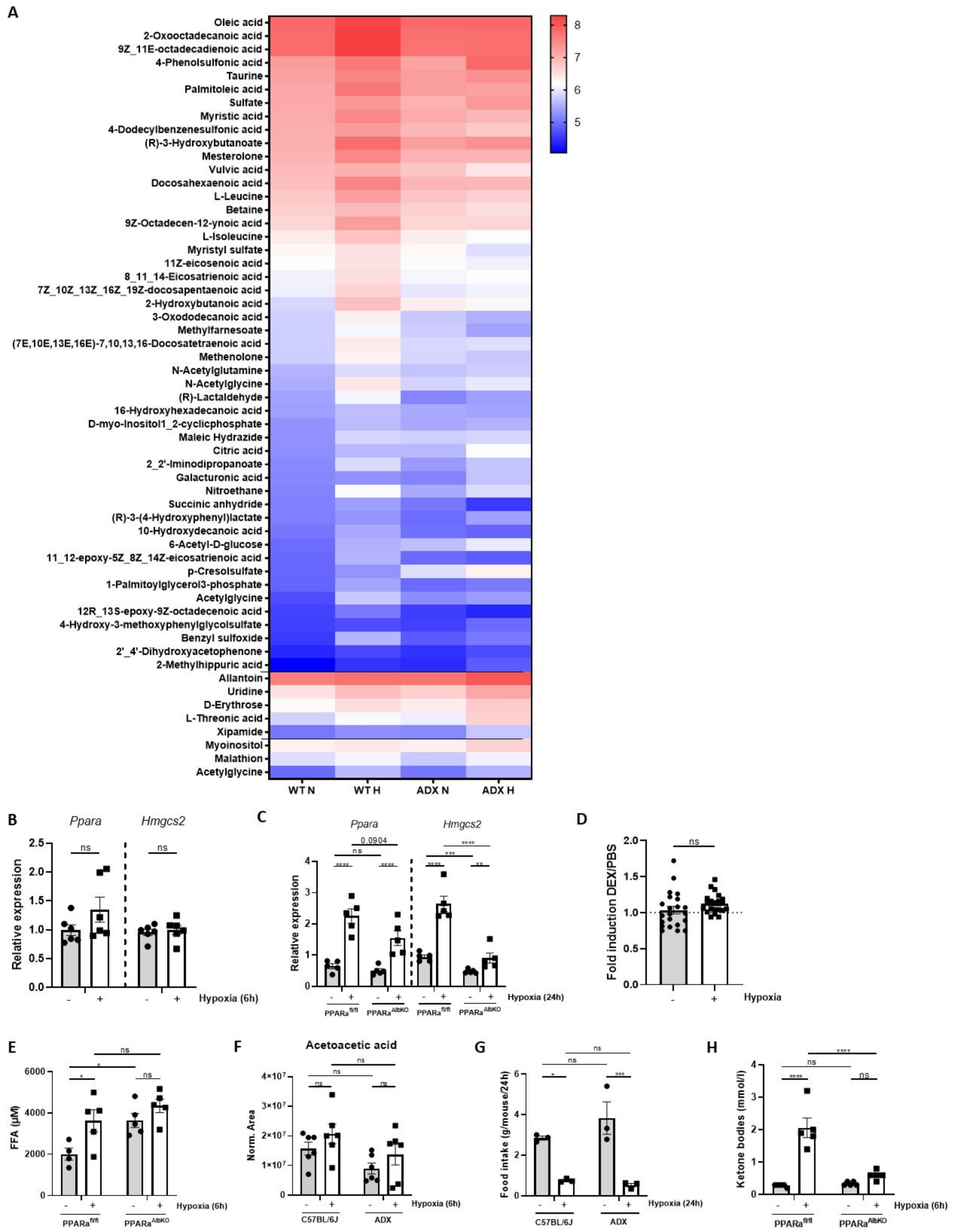


Figure EV5: GR shows attenuated anti-inflammatory capacity under hypoxic conditions

